2014

High-Strain Rate Tensile Characterization Of Graphite Platelet Reinforced Vinyl Ester Based Nanocomposites Using Split-Hopkinson Pressure Bar

Brahmananda Pramanik
University of Mississippi

HIGH-STRAIN RATE TENSILE CHARACTERIZATION OF GRAPHITE PLATELET REINFORCED VINYL ESTER BASED NANOCOMPOSITES USING SPLIT-HOPKINSON PRESSURE BAR

A Dissertation
presented in partial fulfillment of requirements
for the degree of Doctor of Philosophy
in the Department of Mechanical Engineering
University of Mississippi

by

BRAHMANANDA PRAMANIK

October, 2013

ABSTRACT

High-Strain Rate Tensile Characterization of Graphite Platelet Reinforced Vinyl Ester Based Nanocomposites Using Split-Hopkinson Pressure Bar

- Brahmananda Pramanik, Mechanical Engineering, University of Mississippi.

The dynamic response of exfoliated graphite nanoplatelet (xGnP) reinforced and carboxyl terminated butadiene nitrile (CTBN) toughened vinyl ester based nanocomposites are characterized under both dynamic tensile and compressive loading. Dynamic direct tensile tests are performed applying the reverse impact Split Hopkinson Pressure Bar (SHPB) technique. The specimen geometry for tensile test is parametrically optimized by Finite Element Analysis (FEA) using ANSYS Mechanical APDL®. Uniform stress distribution within the specimen gage length has been verified using high-speed digital photography. The on-specimen strain gage installation is substituted by a non-contact Laser Occlusion Expansion Gage (LOEG) technique for infinitesimal dynamic tensile strain measurements. Due to very low transmitted pulse signal, an alternative approach based on incident pulse is applied for obtaining the stress-time history. Indirect tensile tests are also performed combining the conventional SHPB technique with Brazilian disk test method for evaluating cylindrical disk specimens. The cylindrical disk specimen is held snugly in between two concave end fixtures attached to the incident and transmission bars. Indirect tensile stress is estimated from the SHPB pulses, and diametrical transverse tensile strain is measured using LOEG. Failure diagnosis using high-speed digital

photography validates the viability of utilizing this indirect test method for characterizing the tensile properties of the candidate vinyl ester based nanocomposite system. Also, quasi-static indirect tensile response agrees with previous investigations conducted using the traditional dog-bone specimen in quasi-static direct tensile tests. Investigation of both quasi-static and dynamic indirect tensile test responses show the strain rate effect on the tensile strength and energy absorbing capacity of the candidate materials. Finally, the conventional compressive SHPB tests are performed. It is observed that both strength and energy absorbing capacity of these candidate material systems are distinctively less under dynamic tension than under compressive loading. Nano-reinforcement appears to marginally improve these properties for pure vinyl ester under dynamic tension, although it is found to be detrimental under dynamic compression.

DEDICATION

This dissertation is dedicated to all who helped me and guided me through my own times of stress and anxiety. In particular, I dedicate my work to my mother, Mrs. Monomaya Pramanik who showed me the light of life and my elder siblings who raised me in absence of my father since childhood. I thank my beloved wife, Bulbul Majumder, M.S. in Engineering Science and my cuddly son, Indro Aiden Pramanik who added more life in my research and kept me focused toward my goal.

ACKNOWLEDGMENTS

This thesis would not have been possible without the continuous support, advice and encouragement of my advisor, Dr. P. Raju Mantena, Professor of Mechanical Engineering. I express my deepest appreciate to my Ph.D. committee members, Dr. Arunachalm M. Rajendran, Chair and Professor of Mechanical Engineering, Dr. Tyrus A. McCarty, Graduate Coordinator and Associate Professor of Mechanical Engineering, and Dr. Ahmad Al-Ostaz, Professor of Civil Engineering. I could not have financed my studies without the Research Assistantship jointly provided by the Office of Naval Research, Solid Mechanics Program (Dr. Yapa D. S. Rajapakse, Program Manager) Grant No. N00014-7-1-1010; US Army Research Office under the DOD-PIRT sub-contracted through North Carolina A & T University Grant No. 300223243A; Teaching Assistantship from Department of Mechanical Engineering and Dissertation Fellowship from Dr. John Kiss, Dean of the Graduate School, University of Mississippi.

I like to thank Dr. Tezeswi Tadepalli, Research Assistant Professor of Mechanical Engineering for his continuous help in conducting SHPB tests in Blast and Impact Dynamics Laboratory; Dr. Lawrence Drzal's group at Michigan State University for producing the vinyl ester based nanocomposite panels for this research; and Mr. Andy Gossett, Machine-shop Supervisor at the University of Mississippi for machining test-specimens and fabricating all components required for developing the experimental set-up.

Lastly, I acknowledge the collegial support from my fellow doctoral and master students, Damian Stodard and Kiyun Kim. You made this part of my life enjoyable and enriching.

TABLE OF CONTENTS

LIST OF TABLES

LIST OF FIGURES

CHAPTER I INTRODUCTION

Investigating high-strain rate material behavior is essential to solve several real-life problems, i.e., automotive crashworthiness, aerospace impacts due to foreign-objects, dynamic structural loading, and defense applications (projectiles/safety-guard interactions etc.). Interest in high-strain rate mechanical behavior of materials has continued to expand during last 60 years, driven by demand of increased understanding of material response in military technologies concerned with ballistics, armors etc. subjected to high-strain rate loading and impact events. Experimental techniques in characterizing the behavior of materials at high rates of strain are concerned with measuring the change in mechanical properties due to variation of strain rate. One of the most widely used experimental configuration for high-strain rate material response measurements is the split-Hopkinson-Kolskey bar conceived by Hopkinson (1914) [1] and later developed by Kolskey (1949) [2]. This experimental set-up is capable of achieving the highest uniform uniaxial stress loading of a specimen at nominally constant strain rates of the order of 1000/s. In each test instance, stress is directly measured using elastic elements (generally cylindrical bars) mounted in series with the specimen of interest. Stress waves are generated through an impact event, and the elastic elements are considered long enough to keep the duration of the loading pulse less than the wave transit time in the bar.

High-strain rate tensile loading situation becomes evident when a crack develops and propagates at wave speed. Harding et al. (1960) [3] first attempted to adapt the Hopkinson-

Kolskey bar for measuring high-strain rate tensile response of the test specimen. Not only the complexity of generating a tensile-loading pulse, but also designing the tensile test specimen geometry and specimen holding fixture requires more involved research. The comprehensive review of the design-history of tensile Hopkinson-Kolskey bar is important in this perspective. Modification of pressure bar ends to accommodate the gripping of complex tensile specimens and complicated tensile stress generation systems need additional care in data reduction from experimental results to extract quantitative material constitutive behavior. Specimen geometry and experimental configuration require modification depending on the material under investigation. Ongoing research at the University of Mississippi is focused on exfoliated graphite nanoplatelet reinforced vinyl ester based composites. Recently these materials are getting more attention in naval ships and defense applications which experience high-strain rate loading. Investigation of the viscoelastic responses of nanoparticle reinforced composites is useful to predict design criteria for test-specimen of these materials subjected to high-strain rate tensile loading. Consequently the design of specimen-geometry is required to be performed by numerical finite element analysis and experimental validation.

Vinyl ester based composites fall in the thermoset category. Thermoset plastics, being inherently brittle at higher rate of loading and due to the size limitation of the test specimen used in split-Hopkinson bar tests, conventional strain gage application on test specimen becomes tedious and difficult for meaningful data acquisition. Developing a procedure for the non-contact optical measurement of specimen deformation at high-strain rates using high-speed photography or other means would be of potential benefit.

Adapting the conventional compression Hopkinson-Kolskey bar test set-up using an alternative indirect approach, such as, the Brazilian disk method, usually used for brittle

materials can also be considered relevant in developing tensile test method for evaluating material behavior at high rates of loading.

1.1. Literature Review

The Hopkinson bar is one of the most versatile methods considered for dynamic material characterization. This technique, first introduced by Hopkinson in 1914 and later modified to utilize the split bar concept by Kolsky in 1949, is used widely for compression, tension, and shear testing. The basic working principle of the Split-Hopkinson Pressure Bar (SHPB) is that an impact occurs on one end of the incident bar. This produces a loading pulse that propagates along the length of the incident bar, loads the specimen, and then propagates along the transmitter bar. At the incident bar-specimen interface, part of the loading pulse is reflected back down the incident bar. The strain histories of the incident, reflected, and transmitted pulses can be recorded and used to deduce the stress, strain, and strain rate of the specimen using classical one-dimensional elastic-wave-propagation theory [2].

The principles and the data analysis for the tensile split-Hopkinson pressure bar are similar to the traditional compression SHPB. The primary differences are the methods of generating a tensile-loading pulse, specimen geometry, and the method of specimen installation. Last 50 years, several researchers attempted different loading mechanisms to generate tensile pulse in the test specimen. Tensile test specimen geometry has evolved depending on the loading mechanism, dynamic mechanical response of the material, machineability toward specimen preparation and for obtaining meaningful high-strain rate material response. The most popular and technically noteworthy research which has the potential for developing more improved test configuration and specimen geometry are discussed here. Some of these relevant design and

concepts will be adapted for developing test method for evaluating material behavior at high rates of tensile loading.

1.1.1. Methods of tensile pulse generation

The earliest tension version [3] of the Hopkinson bar technique involves generating a compression pulse in a tube surrounding a solid inner rod. The setup is shown schematically in

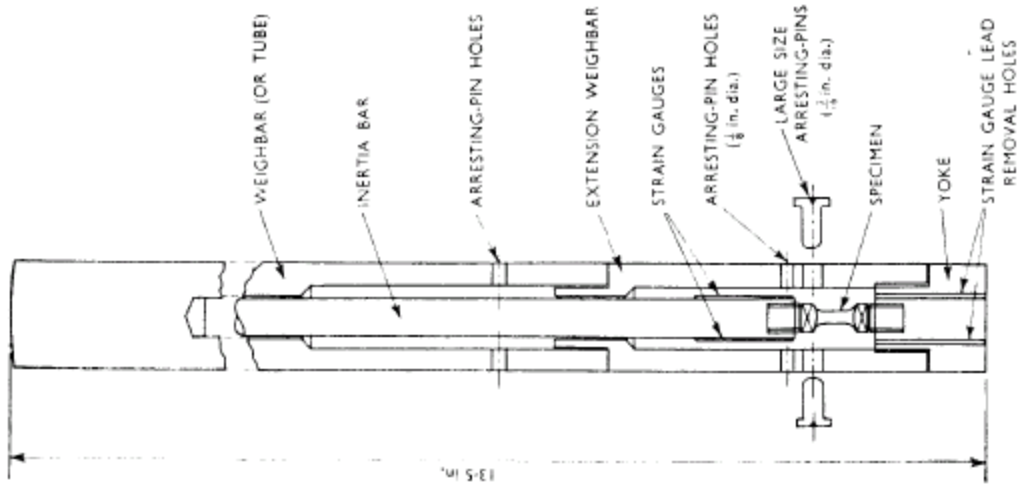

(a)

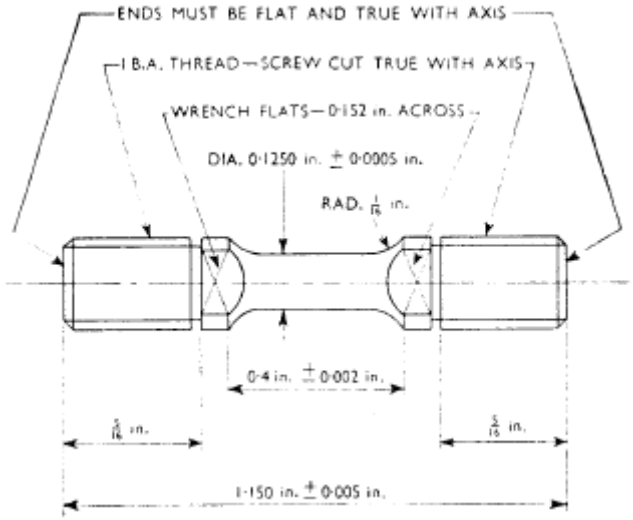

(b)

Figure 1.1: Tensile test set-up using tubular compression bar surrounding the traditional SHPB (a) specimen compression-bar assembly, and (b) test specimen [3]

Figure 1.1-a. The compression tube and SHPB are connected by a mechanical joint shown on the right hand side in Figure 1.1-a. When the compression pulse in the outer tube reaches the joint, which is a free end, the pulse reflects back through the solid inner rod (SHPB) as a tensile pulse. A threaded tensile specimen (Figure 1.1-b) is attached to the inner rod (incident bar) to provide the mechanical connection necessary to transfer the tensile pulse through the specimen and into a second rod (transmitter bar). A tensile version of the split-Hopkinson bar is thus achieved. Although this is a relatively simple method for generating high-strain rate data in tension, the technique suffers from the inability to generate tensile waves having very short rise times because of the wave dispersion at the mechanical joint.

Another unique approach [4] of generating tensile pulse is that the specimen is made like hat, fitting between a solid cylindrical incident bar and a tubular transmitter bar as shown in

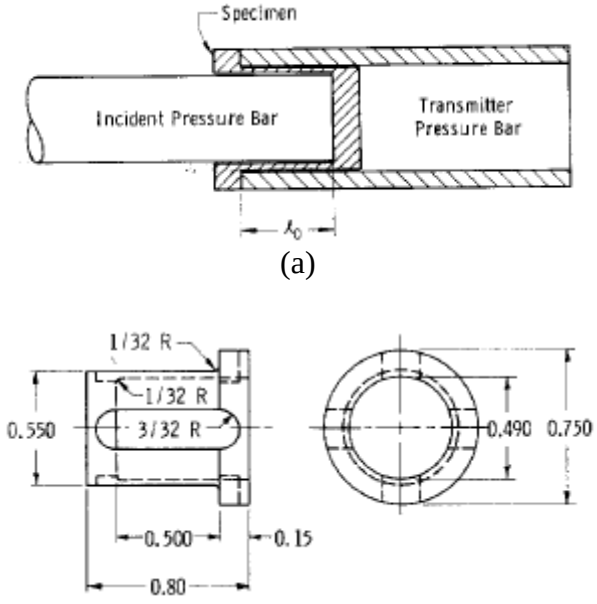

Figure 1.2: Tensile test set-up using tubular transmitter bar and hat-shaped specimen (a) Specimen installation, and (b) Test specimen [4]

Figure 1.2. The actual gage section of the tensile specimen has four equal arms, each with a length-to-weight ratio of approximately 2 to 1. Compression pulse from incident loads the top of hat-shaped specimen and reflects back as tensile wave from the free-end. The tensile pulse passes through four tension arms and reaches to the other end of the specimen. This free-end reflects back this tensile pulse as compression pulse and transmits along the tubular transmitter bar. Although the test is easy to perform, the specimen design requires considerable machining.

Albertini and Montagnani [5] introduced explosive in the process of tensile pulse generation. In this method the explosive is placed in two fire chambers (Figure 1.3) which are symmetrical to the bar. The pressure wave passes through a buffer, which reduces the maximum peak due to the detonation, and transforms the impulse into a larger one, with a reduced maximum value. On reaching mass 1, the wave induces in the bar a tension pulse whose dynamic behavior is determined by both mass 1 and 2. Test specimen is used same as threaded configuration. Only the difficulty of generating pulses with explosives prevents this test

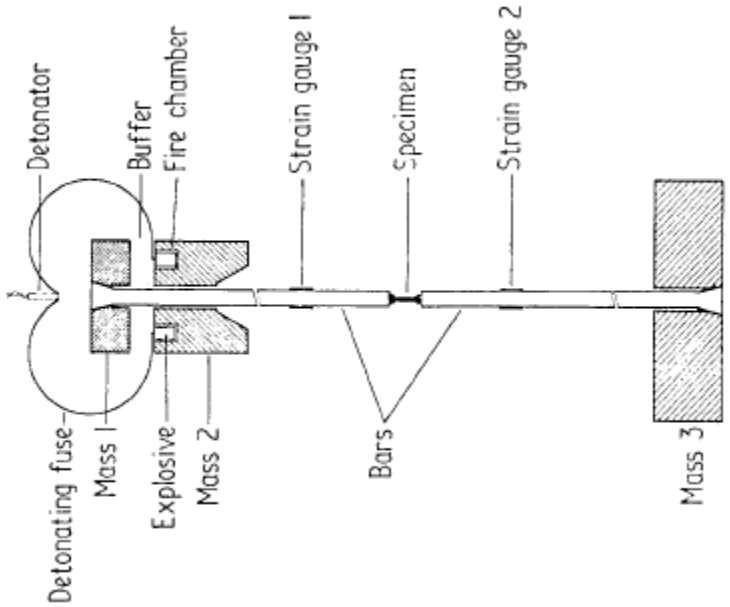

Figure 1.3: Tensile test set-up using explosive [5]

configuration from being a convenient and easily used laboratory apparatus for high-rate tensile testing.

A pre-stressed incident bar was used [5, 6, 7] as an excellent alternative for generating tensile pulse. In this device, the tensile energy stored inside a pre-stressed bar is transferred to the test bar, which is in fact a continuation of the pre-stressed bar, when a brittle intermediate piece blocking off the pre-stressed bar is broken (Figure 1.4). The pre-stressing is applied by a double-screw differential device, or by means of a hydraulic piston. The fracture device consists of a strong tooth, connected to the bar, which causes fracture of the intermediate piece once the desired stress level has been reached. The rupture is provoked by the force exerted by the pre-stressed bar. In such a system, the way the brittle piece breaks or the clamp releases is difficult to control. Therefore, pulse shaping in these systems is not feasible.

The use of a split shoulder surrounding a specimen for introducing the tensile pulse was first shown by Nicholas [8]. This version of a tensile Hopkinson bar uses a threaded specimen

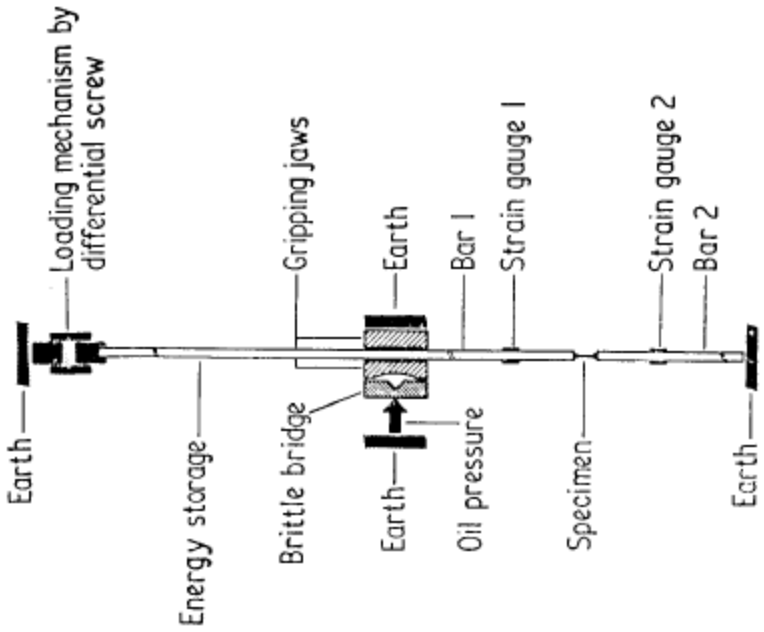

Figure 1.4: Tensile test set-up using pre-stressed incident bar [5]

and a unique split-shoulder arrangement (Figure 1.5-a). The compressive pulse travels down the incident bar until it reaches the specimen. The threaded tensile specimen (Figure 1.5-b) is attached to the two pressure bars. After the specimen has been screwed into the two bars, a split shoulder or collar is placed over the specimen is screwed in until the pressure bars are snug against the shoulder. The shoulder is made of the same material as the pressure bars, has the same outer diameter and has inner diameter just sufficient to clear the specimen. The

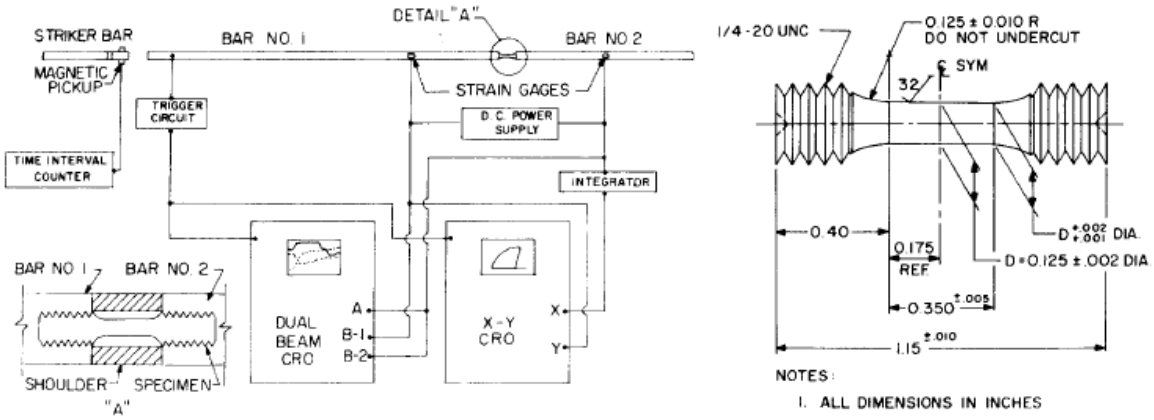

(a) (b)

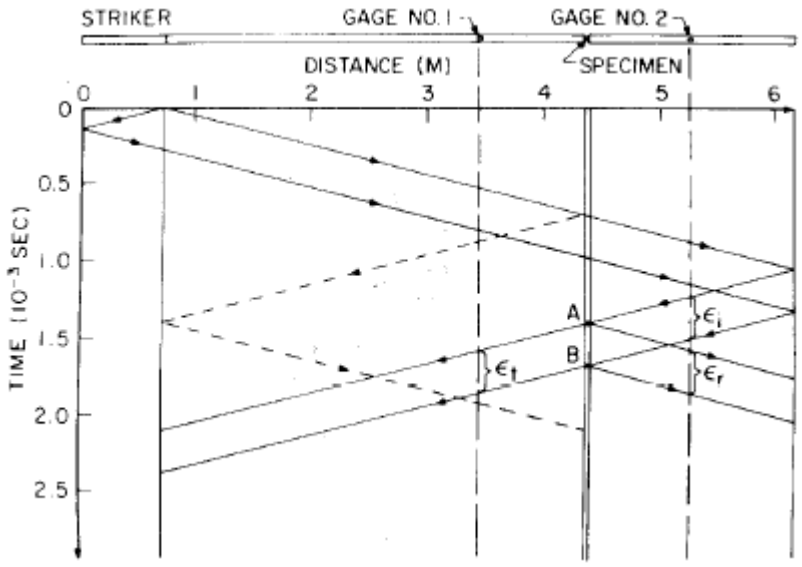

(c)

Figure 1.5: Tensile test set-up using a split shoulder surrounding the specimen (a) experimental set-up, (b) test specimen, and (c) Lagrangian X-T diagram [8]

compression pulse travels through the composite cross-section of shoulder and specimen in an essentially undispersed manner and continues to propagate until it reaches the free end of the transmitter bar (shown in Figure 1.5-c with Lagrangian diagram). There, it reflects and propagates back as a tensile pulse. The tensile pulse is partially transmitted through the specimen and partially reflected back into the transmitter bar. The shoulder, which carried the entire compressive pulse around the specimen, is unable to support any tensile loads because it is not fastened in any manner to the bars. The snug fit of both the shoulder and the threaded specimen against the bars is critical and the most difficult to achieve in the success of this design. Failure of these criteria may cause significant wave dispersion in transmitting compressive pulse by the shoulder and uneven tensile loading of the specimen along with spurious wave reflections.

Another approach [9, 10] to generate direct tension in the incident bar is to strike a flange at the end of the incident bar with same form of kinetic energy. One way to generate the kinetic energy is to use a rotating disk loading system with impact hammers. Figure 1.6 show a schematic of such a loading system in a Kolskey tension bar. Before the disk is accelerated, the

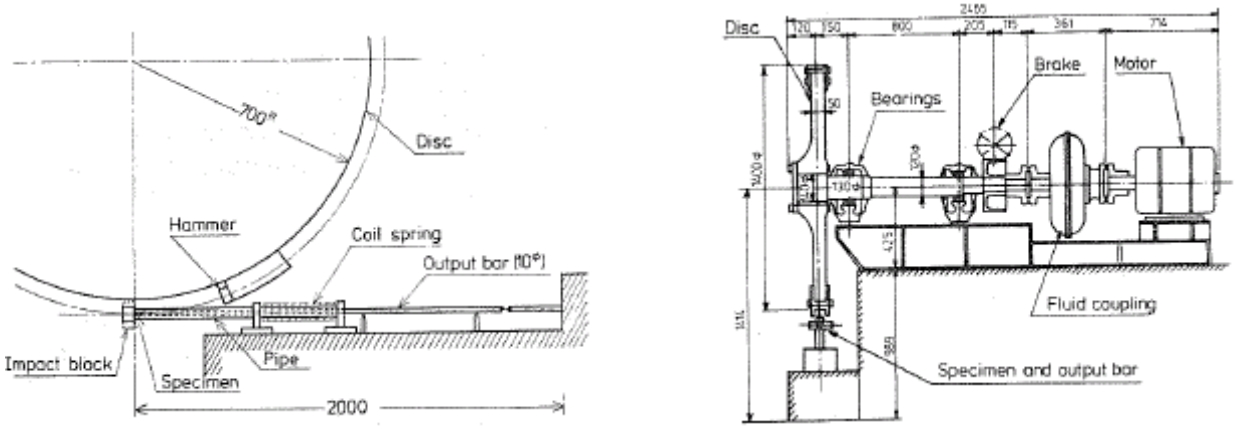

(a) (b)

Figure 1.6: Tensile test set-up striking a flange of incident bar by a hammer (a) Stress-measuring instrument, and (b) corresponding side-view [9]

hammers are retracted into the disk through a caging device. An electromagnetic controller releases the hammers when the disk is rotating at the desired speed, subjecting the hammers to impact on the block which is connected to the incident bar with a prefixed metal bar, as shown in Figure 1.6. The prefixed metal bar is thus stretched to fracture, generating a tensile pulse in the incident bar. The prefixed metal bar provides a means for pulse shaping. With the proper use of

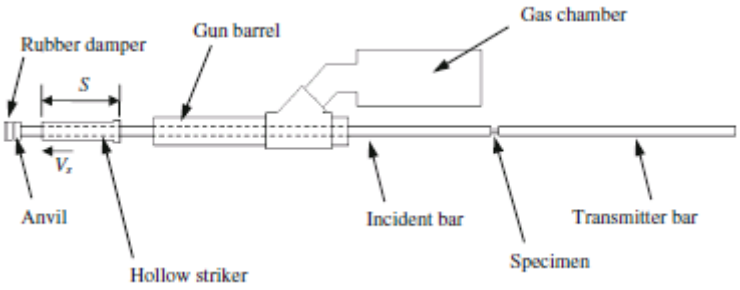

(a)

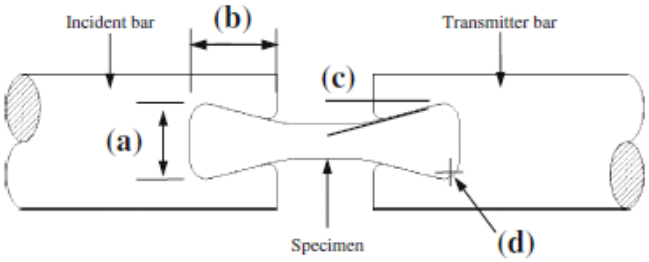

(b)

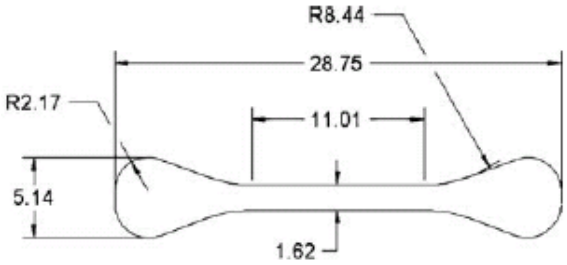

(c)

Figure 1.7: Tensile test set-up striking a flange of incident bar by a tubular striker (a) Test set-up, (b) Specimen assembly, and (c) Specimen geometry [11]

the material and geometry of the bar, the shape of the incident pulse can be controlled to some extent. This tensile setup is capable to conduct dynamic experiments under single and multiple tension loads.

Owen and Tippur [11] used a tubular striker bar for striking a flange of incident bar in reverse direction. This set-up uses a hollow striker riding along the incident bar to produce the tensile load. The striker is accelerated by releasing the air pressure in the gas gun chamber. This translates along incident bar which passes through the barrel of the gas gun. The loading pulse is produced when the striker impacts the flange at the end of the incident bar. Figure 1.7-a shows a schematic diagram of such a system. The apparatus uses a specimen gripping configuration (Figure 1.7-b, c) which does not require fastening and/or gluing and can be readily used for cast-able materials. This mechanism is highly significant for testing particle reinforced polymer composites. On the other hand, this gripping mechanism does not assure if the bar-specimen contact surface perpendicular to the wave propagation remains in contact during the tensile impact. Hence in this case, data reduction using one-dimensional wave propagation theory is questionable.

Specimen installation by cementing to the bar ends [12] was assumed to avoid the complexity of the specimen geometry and to simplify the corresponding wave propagation through the specimen-bar interface. The split-Hopkinson bar apparatus, shown schematically in Figure 1.8-a, is made up of two aluminum bars. The specimen is placed cemented between the bars. The SHB technique used in this case is similar to that described in Reference [6]. A very short cylindrical specimen, as shown in Figure 1.8-b, is used in the tests with the split-Hopkinson bar apparatus. The specimen coupons are glued into two cylindrical aluminum adapters. For use in the split-Hopkinson bar, the unit (a specimen glued to two adapters) is cemented between the

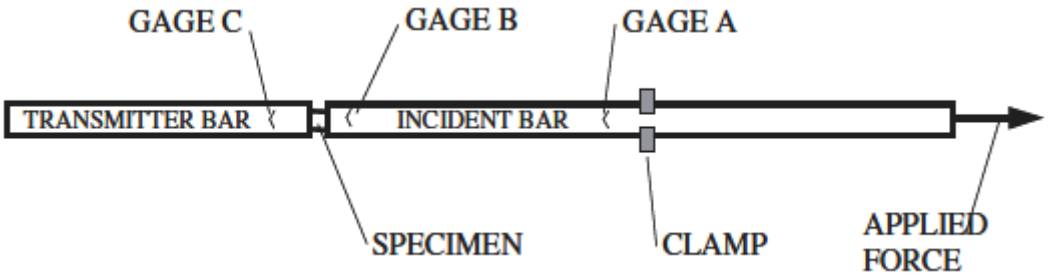

(a)

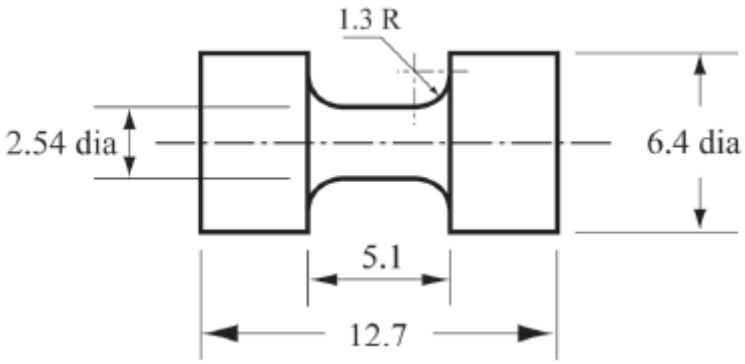

(b)

Figure 1.8: (a) Split-Hopkinson bar apparatus with cemented specimen, and (b) short cylindrical specimen [12]

incident and transmitter bars. This method of installing specimen ensures that the specimen ends are always in contact with the bar ends. This helps to simplify the data analysis. Though, the weaker cementation may spoil the test by unexpected splitting of bar and specimen, or may interfere the wave propagation through the specimen.

An indirect tensile testing method [13] is designed to measure the full dynamic tensile stress-strain curve of low strength brittle solids (shown in Figure 1.9) compiling traditional Brazilian test method with conventional SHPB. The Flattened-Brazilian Disk (FBD) sample is subjected to dynamic load with modified SHPB system. Low amplitude dynamic loading forces are measured by a piezoelectric force transducer which is embedded in the transmitter bar. The

evolution of tensile stress at the center of the disc sample is determined via finite element

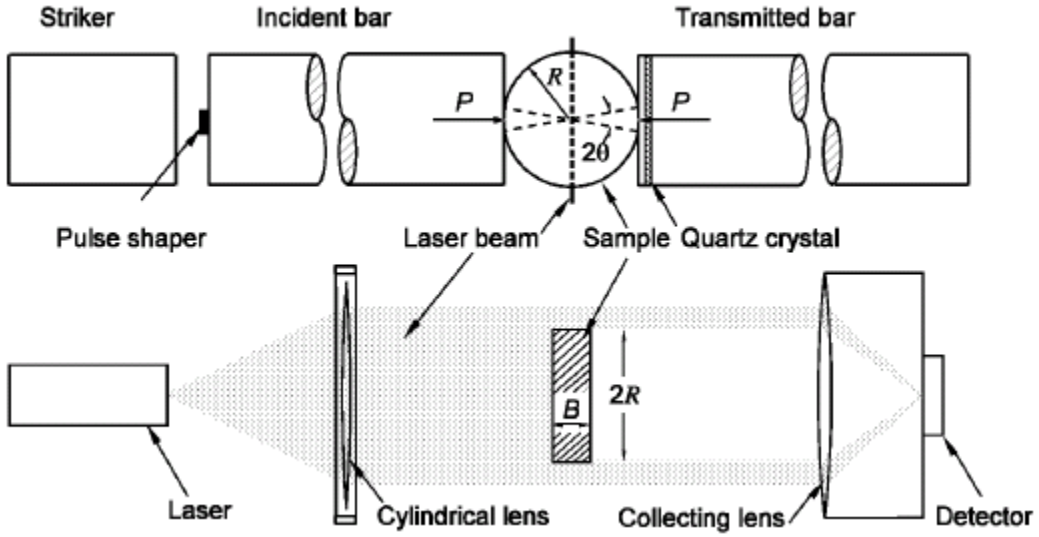

Figure 1.9: Indirect tensile testing using Brazilian disc specimen [13]

analyses with the measured stress in SHPB inputs. In a traditional Brazilian method, a strain gauge is mounted at the center of the specimen to measure the tensile strain, which is difficult to apply for low strength brittle materials. Therefore, a Laser Gap Gauge (LGG) is used to monitor the expansion of the disk perpendicular to the loading axis, from which the average tensile strain is deduced.

1.1.2. Measurement of specimen deformation

Very small strains are developed in relatively brittle materials such as ceramics and thermoset polymeric composites, and so strain gages on the specimen are often required in experiments with these materials. Indeed, several researchers who study ceramics and composites routinely apply strain gages directly to the specimen. However, the application of strain gages directly on each small specimen is a comparatively expensive and time-consuming

process. A direct non-contact measure of the specimen strain would be of great significance under these circumstances.

A photographic system using a Light Eliminating Diode (LED) illuminator and a 35-mm rotating drum camera has been developed [14] for the split-Hopkinson tension bar. Back-lit photographs of deforming tensile samples are obtained at rates up to 50 kHz. The LED exposures are precisely time-correlated with the conventional bar-strain gauge records. The system can be used to extend the measurement of stress-strain curves beyond the onset of plastic instability (necking).

High-speed photography is being extensively used in high-strain rate tensile tests. During the tearing process of a steel specimen [15] due to the tensile pulse (Figure 1.10-a), a series of high speed digital frames are captured of the ligament being deformed (Figure 1.10-b), using a high speed image converter camera (ULTRANAC). The exposure time is generally 0.4 μs and the interval between two consecutive frames is 2-3 μs, depending on impact velocity. The camera is equipped with a long distance microscope lens making it possible to study an area of approximately 1.5×1.5 mm^2 with a stand-off distance of about 100 mm. A high voltage electrical discharge from a capacitor is used to illuminate the target. The duration of the discharge is sufficiently long to cover the entire tearing event. A strain gauge on the loading rod is used as triggering devise. The amplified signal triggers the transient recorder. After a time delay which is adapted to the travel time for the wave in the loading rod, also the flash and the high speed camera are fired. Time-history of displacement of the ligament left end evaluated from high speed photographs is shown in Figure 1.10-c. A detailed description of the use of photographic information for obtaining the time history of the ligament extension is given in [15].

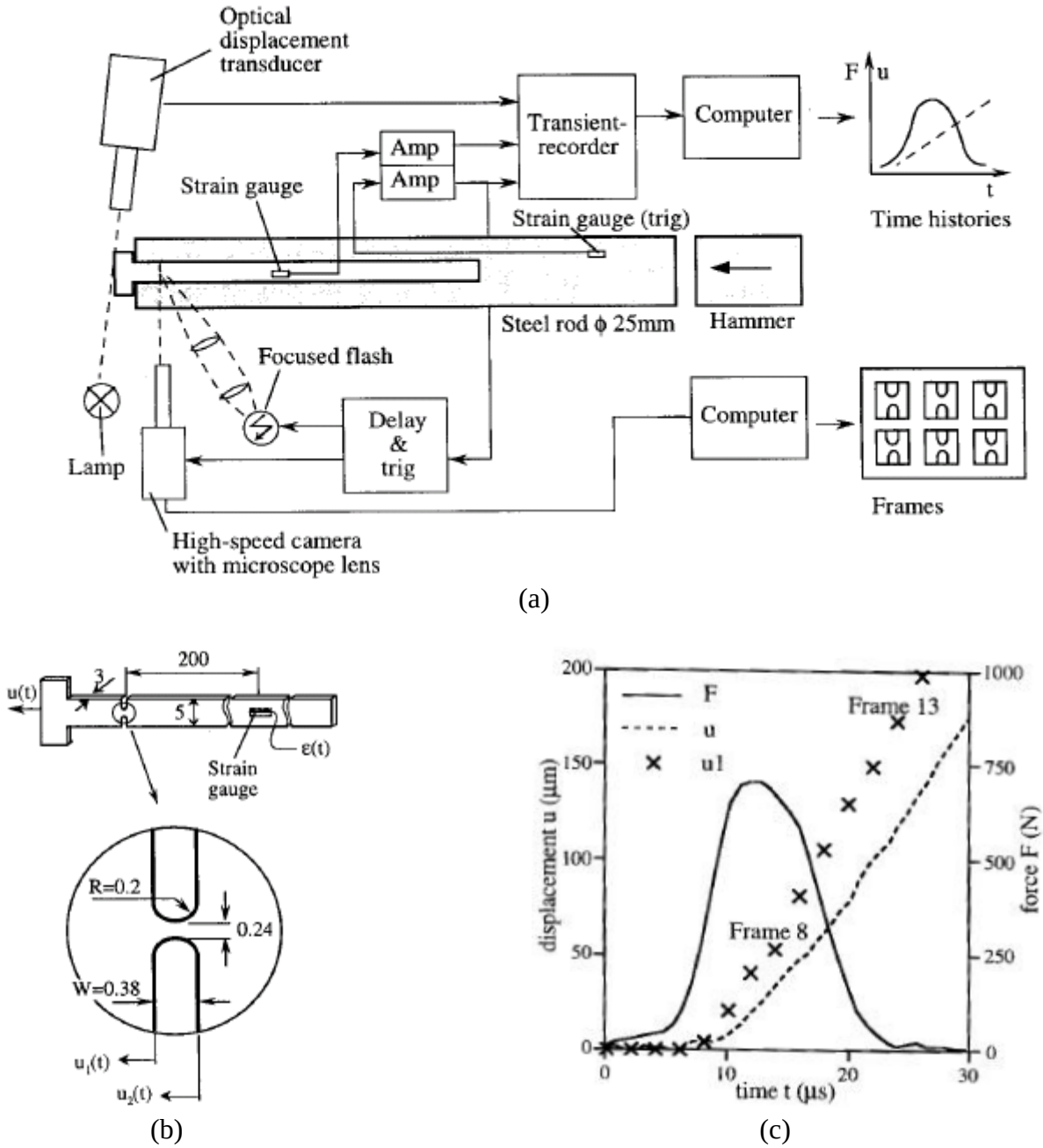

Figure 1.10: Application of high-speed photography in tensile Hopkinson bar tests (a) Experimental set-up, (b) Specimen geometry, and (c) Time-history of displacement ('x'- line) of the ligament left end evaluated from high speed photographs [15]

The Imacon-468-MK II digital CCD camera, manufactured by Hadland Photonics, is used [16] with the viscoelastic SHPB technique to study soft material behavior under dynamic loading

conditions. The camera was set to trigger off the incident strain pulse from the SHPB setup, send a flash command to a light unit, and begin taking a timed sequence of pictures at a given time from the initial signal. The versatility of the image timing allowed a series of real-time photographs to be taken from a single experiment, capturing different specimen strains. The camera's imaging software is also capable of being calibrated from a known distance on an image in order to record measurements. A small plastic scale was attached to the transmitted bars near the specimen-bar interface, to facilitate calibration. This allowed the determination of specimen axial (length) as well as transverse (diametral) dimensions as a function of time during the dynamic loading process. The image analysis software of the camera was then utilized to determine the specimen axial and transverse strains.

1.2. Material description

Vinyl ester based composites are used in applications such as pipelines and chemical storage tanks and also being considered for ship hulls. Figure 1.11 shows the idealized chemical structure of a typical vinyl ester. As the reactive sites are positioned only at the ends of the

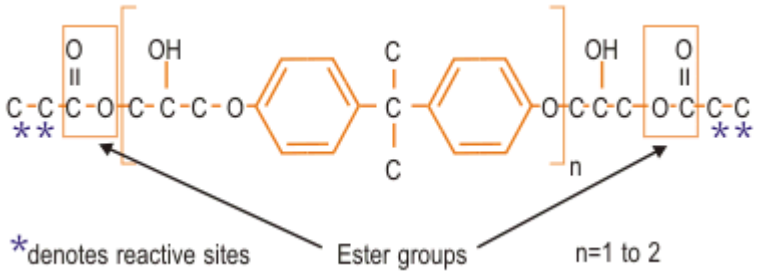

Figure 1.11: Chemical structure of a typical epoxy based vinyl ester [17].

molecular chains, the long molecular chain makes vinyl ester resin tough and resilient to shock loadings (to some extent). The ester groups in the molecular structure are susceptible to water

degradation by hydrolysis. The vinyl ester molecule features fewer ester groups, hence, exhibits better resistance to water and to some chemicals [18, 19]. Several attempts [18-31] have focused on improving the mechanical properties of vinyl ester composites by providing reinforcement. Graphite nanoplatelet reinforcement and toughening with CTBN liquid-rubber agent have been recently considered for this composite system.

Vinyl ester resin offers significant mechanical toughness and excellent corrosion resistance. DERAKANE 510A-40 vinyl ester was considered as the polymeric matrix for nanocomposites in this research work. Brominated DERAKANE 510A-40 is a mixture of 38 wt. pct. styrene and 62 wt. pct. brominated bisphenol-A based vinyl ester. Styrene allows the chain extension because of its single unsaturated carbon-carbon double bond, while the vinyl ester resin with two reactive vinyl end groups enables the cross-linking for network. It is modified to produce the maximum degree of fire retardancy combined with enhanced chemical resistance and toughness on addition of Butanone peroxide, N,N-Dimethylaniline, Cobalt Naphthenate, and 2-4-Pentanedione as additives [31]. DERAKANE 510A–40 resin is believed to provide outstanding resistance to caustic alkalis, hypochlorite bleaching chemicals and hot water, as well as, corrosion resistance. It is used extensively in FRP ductwork, stacks, and stack liner applications, handling mixtures of air and hot gases or potentially flammable liquids [18].

Graphite can accept various atoms, ions, and even molecules between its interlayer space of hexagonal layers of carbon atoms through certain chemical and physical treatment methods. This phenomenon is called intercalation [21]. When graphite intercalation compound (GIC) is heated, the GIC induces the vaporization of the intercalated species and a significant expansion of the material along the crystallographic c-axis occurs, while the in-plane lattice constant remains almost unchanged. Depending on the intercalation methods, the heating rate and the

maximum temperature reached, expandable (exfoliated) graphite can lead to volumes expansions as high as 300 times [20]. Exfoliated graphite becomes after thermal expansion, expanded graphite which is a highly porous worm-like structured material. The expanded graphite also has very low densities within the range of $2x10^{-3}$ – $10x10^{-3}$ g/cm^3 [24] and a high surface area of about 40 – 85 m^2/g [25]. Once intercalated and exfoliated by chemical processes, exfoliated graphite possesses high aspect ratios, which is greater than 1000 [22]. Nanocomposites with graphite platelets show additional excellent electrical and thermal conductivity apart from improved strength, modulus, heat distortion temperature, and barrier properties [27]. Nanocomposite materials made with nanographite platelet are shown [28] to have better flexural strength and higher modulus than that of commercially available carbon reinforcing materials like PAN based carbon fiber and Vapor Grown Carbon Fiber (VGCF).

Auad et al. [23] investigated the mechanical behavior of vinyl ester resin cured with styrene and modified with liquid rubber CTBN. A sharp drop in density causing detrimental fracture toughness was observed in higher CTBN concentrations (>10 wt. %). Balakrishnan et al. [29] examined the fracture behavior of rubber dispersed epoxy and inferred cavitations, yielding, plastic deformation of matrix, crack diversion and energy dissipation caused by rubber particles which contribute to the improvement of the ductility of the epoxy nanocomposite system. Frohlich et al. [26] suggested the compatibility matching as the key to novel phase-separated nanocomposites with significantly improved toughness.

This research includes investigation of vinyl ester graphite platelet reinforced composites added with an almost unreactive liquid Carboxy Terminated Butadiene Nitrile (CTBN) rubber, a

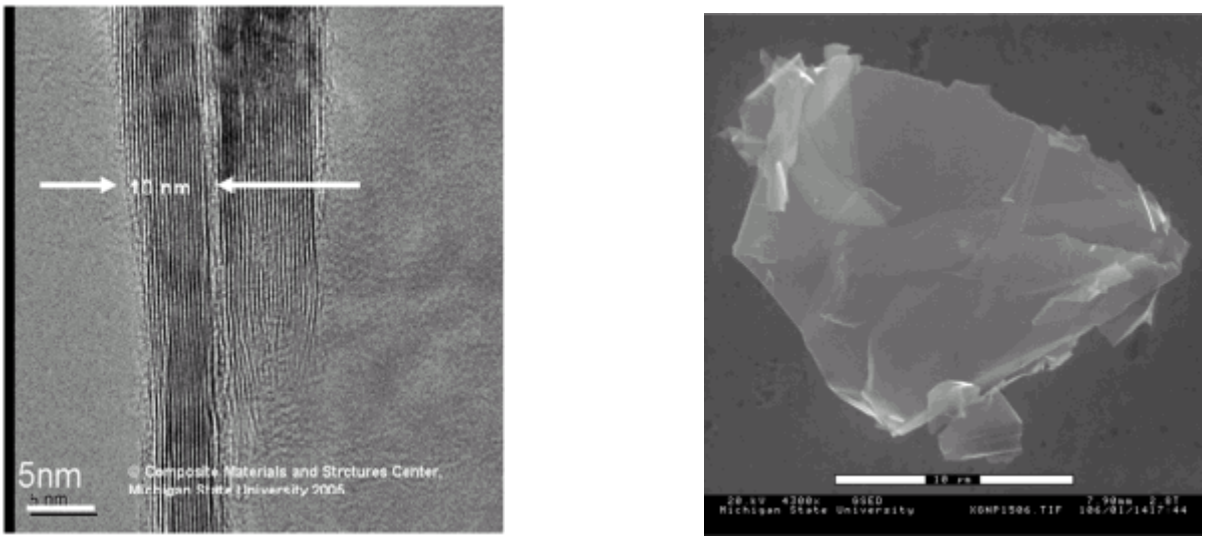

(a) (b)

Figure 1.12: Morphology of nanoparticles dispersion (a) edge view (TEM) of xGnP, and (b) lateral view (SEM) of xGnP [30]

toughening agent for thermoset resins. Exfoliated graphite nanoplatelets (xGnP) were developed at Michigan State University according to the method described in [30]. These xGnP nanocomposites have exfoliated and dispersed graphite platelets with 1 nm thickness and several hundred nanometers width. Distance between layers is in the range of 10~30 Å and size of the layered graphite extends from several hundred nanometers to several microns. Figures 1.12-a and 1.12-b show morphology of xGnP inside a polymer using TEM and SEM.

1.3. Previous work

Ongoing research at the University of Mississippi on developing stronger, safer and more cost-effective structures for the new generation naval ships capable in blast, shock and impact mitigation has accomplished several noteworthy investigations.

1.3.1. Quasi-static tests

Tensile properties were measured using ASTM D 638-08 Standard [31] Test Method for Tensile Properties of Plastics. From the test data, tensile modulus, strength, Poisson's ratio, and effective plastic strain were determined. Three specimens were tested from each of the nanoreinforced vinyl ester composites. Figure 1.13-a shows the specimen specifications and the quasi-static loading in MTS system (Figure 1.13-b).

Tests were conducted [32] under displacement control mode at a strain rate of 0.001/s (displacement rate of 0.05 in/min). Unloading processes were also done to experimentally characterize the permanent plastic strain. The true stress-strain curves at each strain rate along with other properties (density, plastic strain at failure) were determined.

Compressive properties for vinyl ester and its nanocomposites were measured using a combined loading compression [33]. The compressive force was introduced to the specimen by a typical combined loading compression test fixture. This type of fixture is ideally used to test an untapped, straight-sided composite specimen of rectangular cross-section. Specimens with 140 mm (5.5 in) long and 12 mm (0.5 in), with no specific thickness [33] were installed in the fixture. Strain gages were bonded on 26 unsupported 12 mm gage length (both sides), and connected through wires via a strain indicator box. The fixture, which subjects the specimen to a combined end-shear loading, is loaded in compression (0.05 inch/min) between flat platens in a Universal Material Testing System. Load-strain data were collected until a specified strain level (3%) is achieved and not the complete stress-strain curve to failure [32].

The stress-strain responses of the full range of nanocomposites at quasi-static tensile-loading are shown in Figure 1.13-c (Note: these experimental data have been normalized to the respective specimen areal density – NTAD [32, 34]). Quasi-static uniaxial tensile properties for

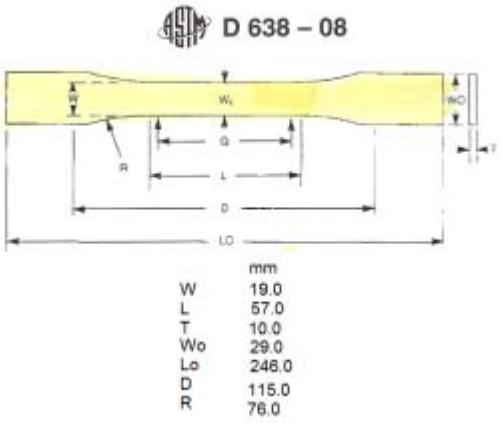

(a)

(b)

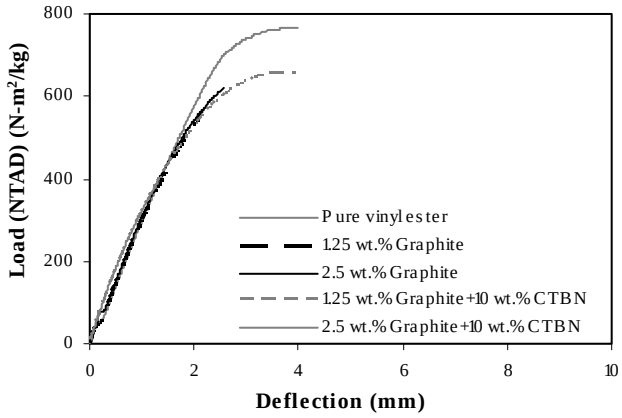

(c)

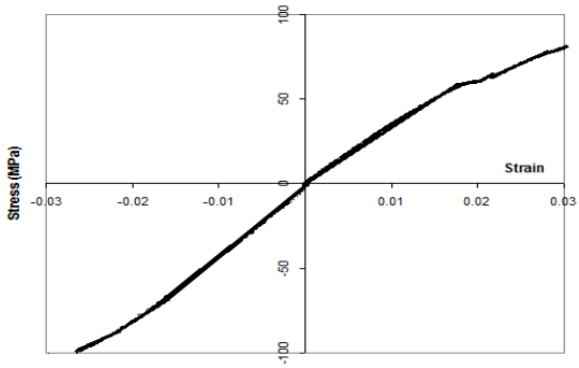

(d)

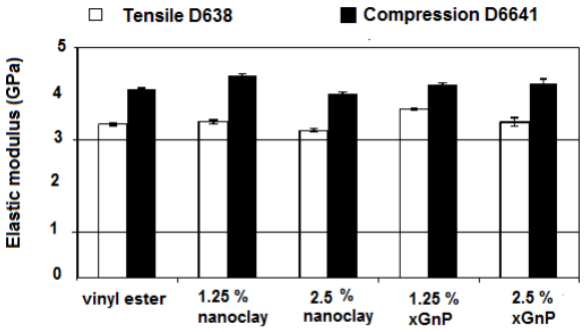

(e)

Figure 1.13: (a) Dimensions of tensile test specimen (ASTM D 638-08), (b) Quasi-static loading in Material Test System (MTS), (c) Tensile test result for vinyl ester nanocomposites, (d) Tension and compression stress-strain data for pure brominated vinyl ester, and (e) Tension and compression modulus (GPa) for vinyl ester nanocomposites [32]

these nanoparticle composites are given in Table 1.1. It shows that the nanocomposite toughened with CTBN is stiffest, though pristine vinyl ester shows highest strength to failure. A typical stress-strain curve with both tension and compression is shown in Figure 1.13-d.

Table 1.1: Quasi-static direct tensile properties of nanocomposites [32] tested according to ASTM 638-08 standard using dog-bone specimen geometry.

Matrix	**Reinforcement**	**Toughening agent**	**Density (kg/m^3)**	**Poisson's Ratio**	**Elastic Modulus (GPa)**	**Strength (MPa)**	**Ultimate strain (%)**
Brominated Vinyl ester	None	None	1338	0.37	3.49	81.5	3.14
Brominated Vinyl ester	1.25 wt.% xGnP	None	1352	0.35	3.82	39.1	1.28
Brominated Vinyl ester	2.5 wt.% xGnP	None	1363	0.35	3.71	42.6	1.68
Brominated Vinyl ester	1.25 wt.% xGnP	10 wt.% CTBN	1337	0.35	4.68	45.7	1.48
Brominated Vinyl ester	2.5 wt.% xGnP	10 wt.% CTBN	1343	0.38	5.22	26.0	0.61

Figure 1.13-e compares the elastic modulus for brominated nanocomposites under tension and compression. These quasi-static test results show distinctive response in tensile and compressive loading. It indicates that some unique responses can be observed from high-strain rate tensile testing, considered in this dissertation prospectus.

1.3.2. Viscoelastic characterization

A viscoelastic material exhibits viscous and elastic behavior. Elastic material is one which returns all the energy stored during loading after the load is removed [36]. As a result, the stress and strain response for elastic materials moves totally in phase. For elastic materials, Hook's law applies, where the stress is proportional to the strain, and the modulus is defined at

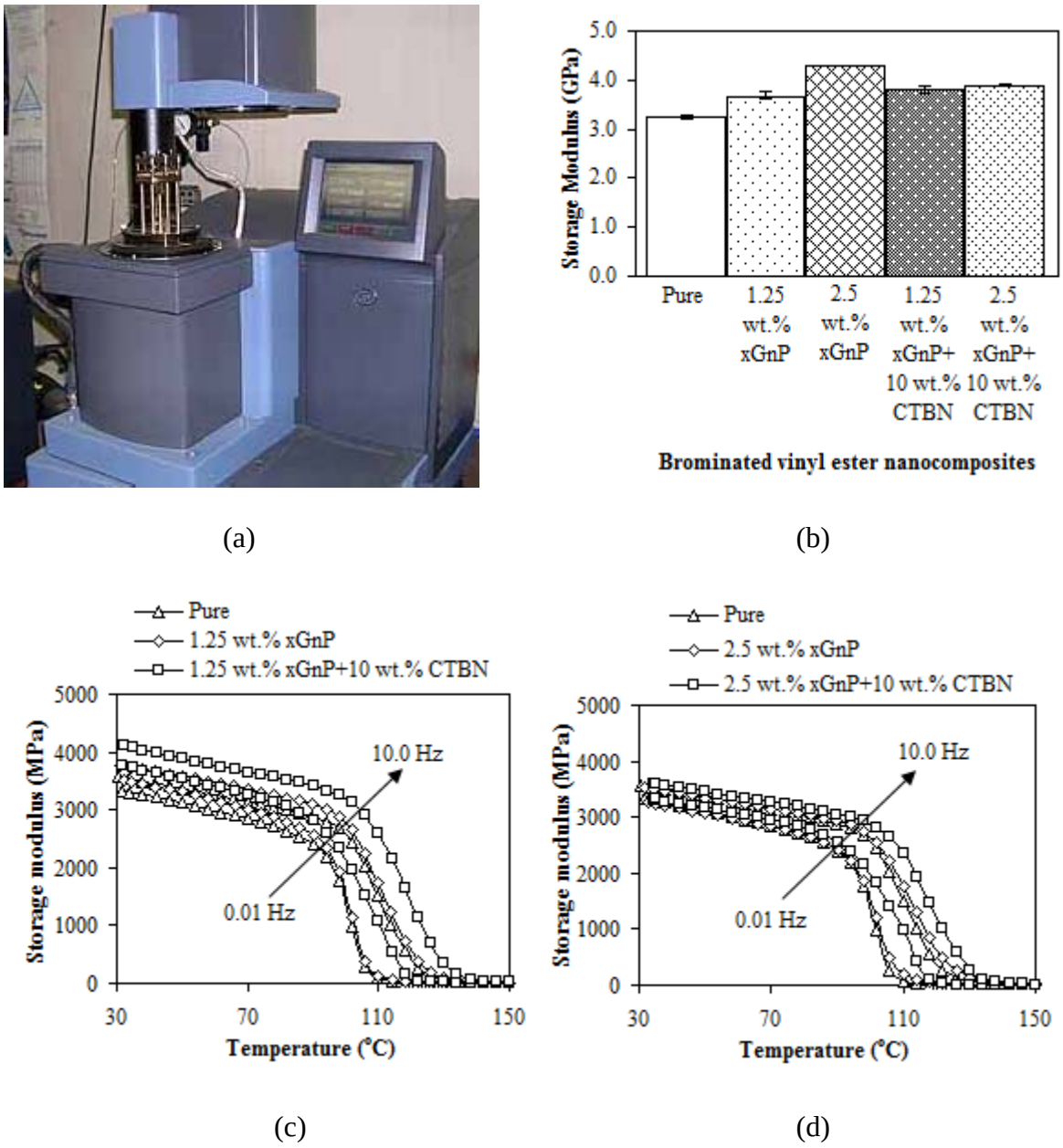

Figure 1.14: (a) TA Instruments Model Q800 DMA for dynamic tests, (b) storage modulus at initial temperature for brominated vinyl ester nanocomposite (c) storage modulus for 1.25wt% reinforced brominated vinyl ester nanocomposites at multi-frequency, and (d) storage modulus for 2.5wt% reinforced brominated vinyl ester nanocomposites at multi-frequency [37]

the ratio of stress and strain. A purely viscous material returns none of the energy stored during loading. All the energy dissipated as “pure bending” once the load is re-moved. In this situation,

the stress is proportional to the strain rate rather than strain. These materials, known as inelastic materials, have only damping, instead of stiffness. Both of these two types are ideal in existence. The materials, which do not fall into any of the above categories, are named as viscoelastic materials. Some of the energy stored in a viscoelastic system is recovered upon removal of the load, and the remainder is dissipated as heat [36]. The viscoelastic modulus is represented by a complex quantity. The real part of this complex parameter, known as storage modulus (E_1), relates the elastic behavior of the material, and defines the stiffness. The imaginary component, known as loss modulus (E_2), explains the material's viscous behavior, and defines the ability of energy dissipation of the material. The complex viscoelastic modulus (E^*) is defined as:

$$E^* = E_1 + iE_2 = \frac{\sigma_0}{\varepsilon_0} e^{i\phi} \tag{1.1}$$

Dynamic Mechanical Analysis (DMA) was performed [37] in accordance with ASTM D4065-01 standard [38]. TA Instruments Model Q 800 DMA (Figure 1.14-a) is a stress-controlled Combined Motor and Transducer (CMT) machine where the motor applies a force and displacement sensors measure strain, force and amplitude in the form of raw signals recorded by the machine [39]. Experiments were performed using the single-cantilever clamp. Hence the most of the strain occurred at the sample surface, while the center experienced no strain. The stress and strain equations (equations 1.2 to 1.5), applied in these experiments, are based on the theory of linear viscoelasticity for material [36, 39]

$$E = \frac{K_S}{F_c} . \frac{L^3}{12I} \left[1 + \frac{12}{5} (1+\upsilon) \left(\frac{t}{L} \right)^2 \right] \tag{1.2}$$

$$F_c = 0.7616 - 0.02713 \sqrt{\frac{L}{t}} + 0.1038 \ln\left(\frac{L}{t} \right) \tag{1.3}$$

$$\sigma_x = \frac{6PL}{wt^2} \tag{1.4}$$

$$\varepsilon_x = \frac{3\delta F_c}{L^2\left[1+\frac{12}{5}(1+\upsilon)\left(\frac{t}{L}\right)^2\right]} \tag{1.5}$$

where, E = elastic modulus, K_s = measured stiffnes, F_c = clamping correction factor, L = clamp span length, I = sample moment of inertia, υ = Poisson's ratio, t = sample thickness, σ_x = stress, P = applied load, w = width of the specimen, ε_x = strain, δ = amplitude of deformation.

The viscoelastic properties, such as, modulus (stiffness) and damping (energy dissipation), of the exfoliated graphite platelet added with CTBN reinforced brominated vinyl ester were studied over a range of temperature and frequency. Creep and stress relaxation experiments were also conducted using DMA [37].

DMA measurements included frequency sweep with time temperature steps, to which time-temperature super-position (TTS) was applied [37] to predict the long-term time dependent properties of the material. The dynamic storage modulus (*E'*) and damping of nanoreinforced brominated 510A-40 vinyl ester specimens were characterized as a function of temperature and frequencies. Dynamic mechanical testing was used to perform multi- frequency measurements with accelerated temperature and theoretical time-temperature superposition post-processing of the data. Effects of CTBN inclusion in exfoliated graphite platelet reinforcement were investigated.

Vinyl ester nanocomposites were characterized by performing a multi-frequency isothermal mode test, in which the sample is equilibrated at different temperatures and subjected to a series of frequencies. Figure 1.14-b shows the detrimental effect of CTBN addition in storage modulus with respect to 12.5 wt% xGnP reinforcement at 30°C. Figures 1.14-c and 1.14-

d show the storage modulus variations with temperature for brominated vinyl ester nanocomposites with the multi-frequency tests. It can be observed that the modulus is increasing with the increase of frequency. Frequency dependent storage modulus indicates strain rate dependent behavior of the nanoparticle composites. Hence the investigation of material properties at high strain rates is important.

1.3.3. Punch-shear tests

The low velocity punch-shear tests were performed [34] using Dynatup 8250 drop weight impact test system (Figure 1.15-a), according to the ASTM D3763 Standard [40]. Specimen clamp assembly consists of parallel rigid steel plates with a 3" (76.2 mm) diameter hole in the center of each. Sufficient clamping force was applied to prevent slippage of the specimen during

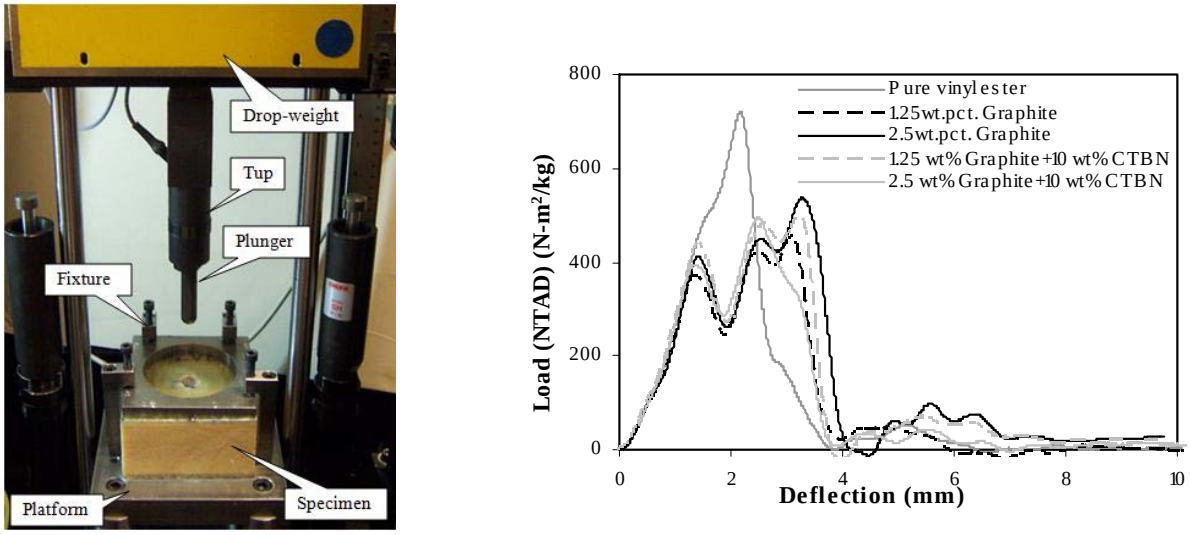

(a) (b)

Figure 1.15: (a) Experimental set-up of low velocity punch-shear test, and (b) Load (NTAD)-deflection response of nanoparticle reinforced composites [34]

impact. Plunger assembly consists of a ½" (12.70 mm) diameter steel rod of 2" (50.8 mm) length

with a hemispherical end of the same diameter positioned perpendicular to, and centered on, the clamp hole. Dynatup Impulse^{TM} data acquisition systems are equipped with load and velocity transducers to provide data collection, analysis and reporting. Using an instrumented tup, the data acquisition hardware captures instantaneous load signals and transfers to the impulse software for further data processing. The velocity at impact is measured just prior to impact using a photoelectric-diode and flag system.

Three samples from each type of nanoparticle reinforced vinyl ester plates, laminated face sheets and sandwich composites were tested under low velocity impact and the average data considered for this investigation. Impact drop weight and height were determined such that velocity slowdown is less than 20% during the impact event as well as the applied impact energy was at least three times the energy absorbed by the specimen at peak load [40]. This configuration provided about 38 J of impact energy and 3.6 m/s impact velocity for the nanoparticle reinforced vinyl ester plates.

Approximately 15 s^{-1} strain rate was achieved during low velocity punch-shear test. The load-displacement responses for the nanocomposites are shown in Figure 1.15-b. This investigation shows that nanoparticle reinforcement helps to absorb more impact energy, and motivates investigation of the material behavior under high-strain rate loading.

1.3.4. Fractal analysis

The fractal dimensions of failure surfaces of vinyl ester based nanocomposites were estimated [41] using two classical methods, Vertical Section Method (VSM) and Slit Island Method (SIM), based on the processing of 3D digital microscopic images. Self-affine fractal

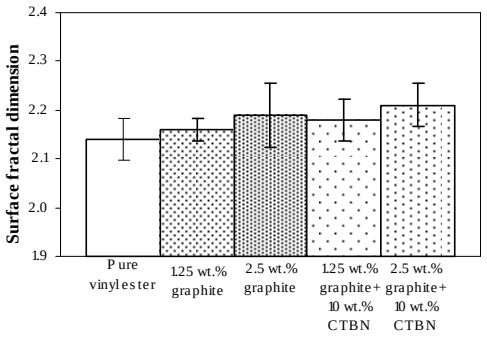

(a)

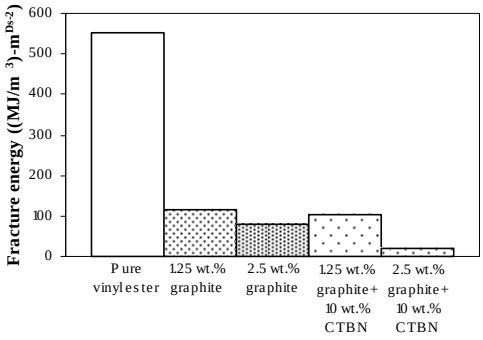

(b)

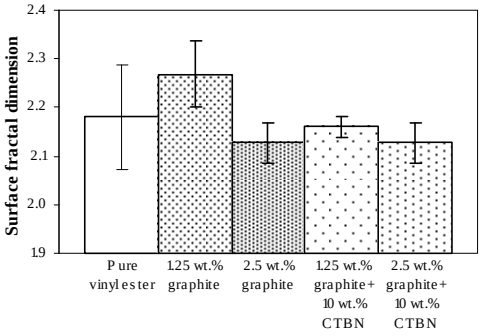

(c)

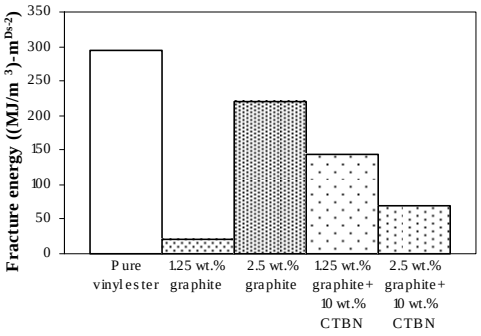

(d)

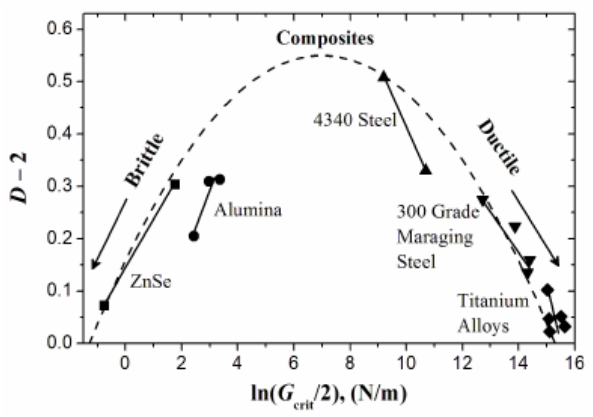

(e)

Figure 1.16: (a) Estimated fractal dimension and (b) fracture energy of nanocomposites tested under quasi-static loading, (c) estimated fractal dimension and (d) fracture energy of nanocomposites tested under low velocity punch-shear, and (e) Relationship between fractal dimension of the fractured surface and fracture energy of different materials [41, 42]

geometry was observed in the experimentally obtained failure surfaces of graphite platelet reinforced nanocomposites subjected to quasi-static uniaxial tensile and low velocity punch-shear loading. Fracture energy and fracture toughness were estimated analytically from the surface fractal dimensionality. Contribution of fracture energy to the total energy absorption of these nanoparticle reinforced composites was demonstrated. For the graphite platelet reinforced nanocomposites, surface fractal analysis depicted the probable ductile or brittle fracture propagation mechanism, depending upon the rate of loading.

The surface fractal dimensionality (shown in Figure 1.16-a) increases with decreasing fracture energy (Figure 1.16-b), for quasi-static tensile loading. This trend is consistent with the ductile response reported in literature [42], and as shown on the right side of Figure 1.16-e. On the other hand, low velocity punch-shear tested specimens illustrate decreasing trend for both surface dimensionality (Figure 1.16-c) and the fracture energy (Figure 1.16-d), which is in agreement with the brittle response shown on the left side of Figure 1.16-e. These two different trends between the fracture energy and surface fractal dimensionality for quasi-static and punch-shear loading are acceptable for composite materials [42]. This indicates rate dependency of the material behavior. The nanoparticle composites show brittle behavior at higher strain rate loading.

These previous observations encourage developing suitable specimen geometry and configuring the Hopkinson bar set-up for tensile testing of the xGnP vinyl ester nanocomposite samples as brittle materials. Adapting the conventional compression Hopkinson-Kolskey bar test set-up using an alternative indirect approach, such as, the Brazilian disc method, (usually used for brittle materials) has been considered in this dissertation work.

1.3.5. Split-Hopkinson Pressure Bar (SHPB) tests

SHPB tests were conducted for graphite platelet/ brominated vinyl ester nanocomposites [35, 43] to obtain the material response (Figure 1.17-a) under compression at a strain rate of approximately 1200 per second at CAVS facility in Starkville, MS under the supervision of Dr.

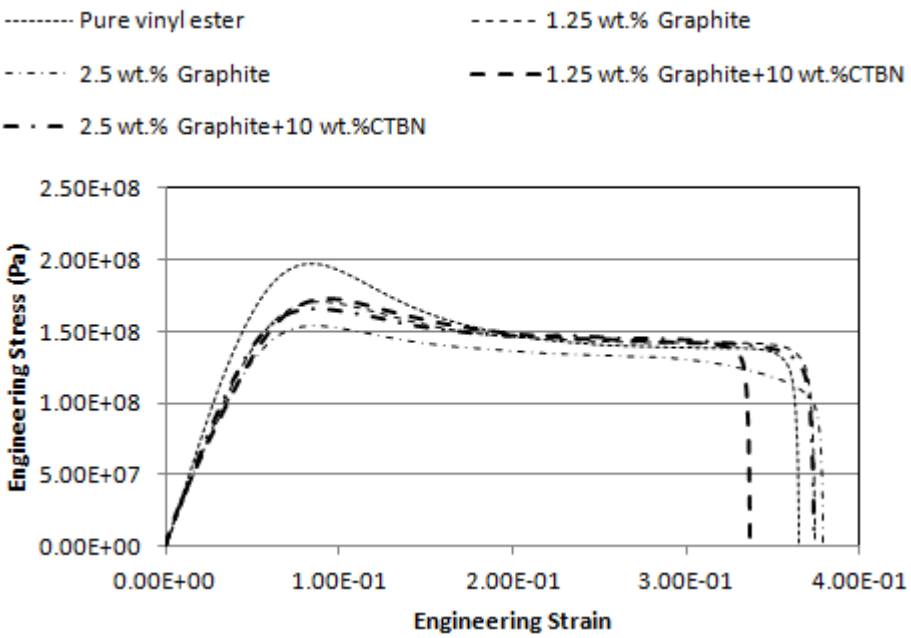

(a)

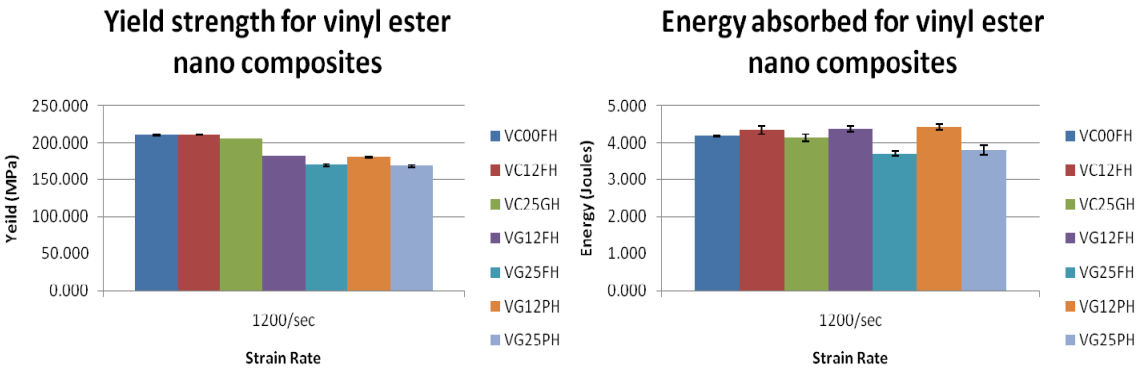

(b) (c)

Figure 1.17: (a) Stress-strain response (b) yield strength, and (c) energy absorption for vinyl ester nanocomposites under high-strain rate (1200/sec) compressive loading (SHPB tests were performed at CAVS facility, Starkville, MS) [34, 42]

D. Hui and J. Lair from University of New Orleans. Small cylindrical specimens cut from the 1.25 and 2.5 wt. pct. nanoclay and graphite platelet reinforced plus the 10% CTBN added brominated vinyl ester plate samples were subjected to high-strain rate compressive loading (~ 1200/sec) in Split-Hopkinson Pressure Bar apparatus. Figure 1.17-b shows that the failure strength of brominated vinyl ester (VC00FH) is reduced with the nanoparticle reinforcement, even with 10 wt.% CTBN added. Absorbed energy (Figure 1.17-c) shows marginal improvement for the 1.25 wt.% graphite platelets (VG12FH) and also with 10 wt.% CTBN added (VG12PH). However, energy absorption decreased with 2.5 wt.% graphite platelets (VG25FH), even with the 10wt.% CTBN added (VG25PH).

The tensile SHPB tests were scheduled at the same facility. The designed specimen geometry (Figure 1.18-a, b) and fixture (Figure 1.18-c) for the test was not successful for obtaining meaningful data. All specimens were failing beyond gage length at the shoulder region. Stress concentration at gripping area and the alignment of the specimen in the fixture are

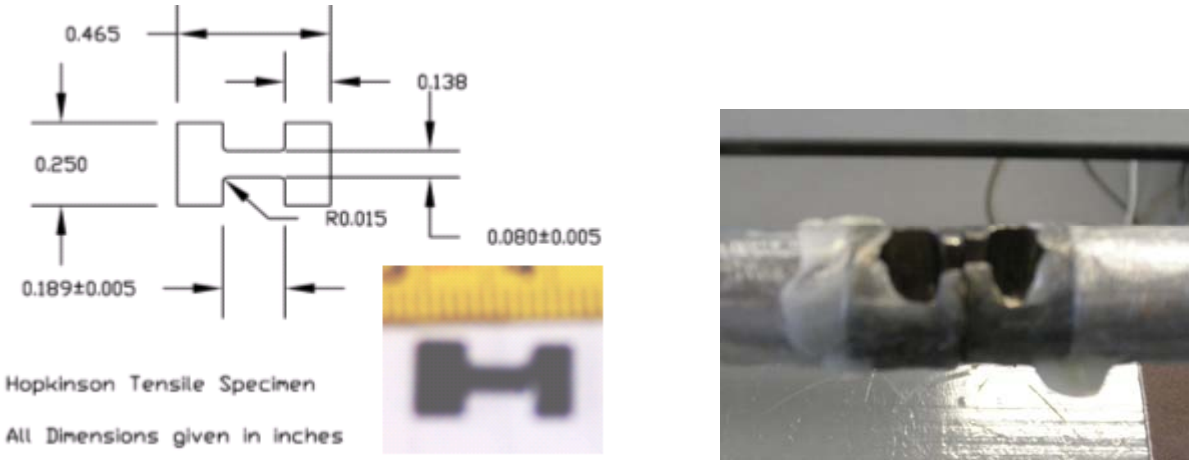

(a) (b) (c)

Figure 1.18: (a) Tensile SHPB test specimen geometry, (b) tensile SHPB test specimen, and (c) tensile SHPB test fixture (SHPB tests were performed at CAVS facility, Starkville, MS) [44]

assumed to be the reason. Re-design of specimen geometry and suitable fixture is has been adopted in this dissertation work for obtaining meaningful high-strain tensile test data.

1.4. Motivation and objective of the research

In previous research conducted [32, 34, 35, 37, 41], it has been observed that the candidate nanocomposite systems are high in stiffness but low in strength, and fail in a brittle fashion. It is observed that the failure of high stiffness and low strength materials is initiated by tensile stress concentrations. Hence the investigation of the high strain-rate tensile as well as compressive response of such materials requires serious consideration. The complexities of generating a tensile-loading pulse, designing the tensile test specimen geometry and holding fixtures have been addressed by multiple researchers [1-16]. Tensile tests on high-stiffness low-strength materials usually considers compression-induced tension in order to avoid pre-mature failure caused from gripping under direct tensile loading. Almost at the same time from opposite sides of the world, Carneiro [45] from Brazil and Akazawa [46] from Japan independently proposed that the circular disk theory (analytically explained [47] by Timoshenko and Goodier) can be applicable in investigating the bearing capacity of a concrete roller. John et. al. [48] reported a similar dynamic splitting tension test method with a compression SHPB for evaluating the effects of strain rate and size on the tensile strength of concrete. The induced tensile strain in the disk specimen can be measured using strain gage mounted on the specimen surface or, alternatively, a high-speed camera combined with digital speckle metrology. Both of these methods are complex in installation, expensive and the data reduction processes are also complicated.

In this investigation, the dynamic response of xGnP reinforced and additionally CTBN toughened vinyl ester based nanocomposites has been determined experimentally under both dynamic tensile and compressive loading conditions. Two different dynamic tensile test techniques are demonstrated and their merits and demerits are compared. Firstly, dynamic direct uniaxial tensile test is performed applying reverse impact SHPB technique. Dog-bone shaped specimen geometry of the tensile test is optimized based on finite element analysis of stress distribution within the specimen and fixture assembly using ANSYS Mechanical APDL®. The stress equilibrium during the dynamic test-event and uniform stress distribution within the specimen gage length is validated using high-speed digital photography. The complex on-specimen stain gage technique for tensile strain measurement is substituted by a non-contact laser occlusion technique. Secondly, dynamic indirect tensile test is performed combining both conventional SHPB technique and Brazilian disk test method. The cylindrical disk specimen is evaluated by traditional Brazilian disk test method combined with conventional SHPB technique. The disk specimen is securely held and self-aligned in two concave-end loading fixtures assembled in between the incident and transmission bars of SHPB system. The complexities of conventional strain gage application on the specimen for measuring the diametrical transverse expansion of the specimen under high-strain rate diametrical compressive loading are eliminated by adapting a non-contact Laser Occluding Expansion Gage (LOEG) technique. The mechanics of this technique is discussed in detail. The diametrical transverse tensile strain is measured using LOEG device. In this case, considering the diametrical gage length is determined to be more convenient than centrally concentrated gage length. High-speed digital photography is performed for diagnosing the specimen failure mechanism and validating the indirect test method for characterizing the tensile properties of graphite platelet reinforced and additionally CTBN

toughened vinyl ester nanocomposites. Finally, conventional compressive SHPB tests are performed and both dynamic tensile and compressive strength and energy absorbing capacity of the candidate material is presented and compared with dynamic tensile response. Finally, the effect of strain rate and the contribution of xGnP reinforcement and CTBN toughening on the tensile properties of vinyl ester based nanocomposites are presented. The effects of xGnP reinforcement and CTBN toughening to the dynamic response of vinyl ester based nanocomposites are investigated.

CHAPTER II EXPERIMENTAL SET-UP

Experimental facilities used in this study consist of a traditional compression and a reverse impact based tension SHPB apparatus. The compression SHPB is combined with conventional Brazilian disk test technique and a Laser Occluding Expansion Gage (LOEG) system for conducting indirect dynamic tensile tests on nanocomposite specimens.

2.1. Material description

Five different DERAKANE 510A-40 [18] vinyl ester thermoset nanocomposites of 10 mm (0.4 inch) thick panels are considered for the dynamic tensile and compressive characterization. The brominated bisphenol-A based vinyl ester consists of 38 weight % of styrene, added with 1% of Butanone peroxide, 0.1% of N, N-Dimethylaniline, 0.2% of Cobalt Naphthenate and 0.2% of 2-4-Pentanedione additives to impart maximum fire retardance, chemical resistance and toughness. The samples were prepared [30] by dispersing about 3000 gm of pure brominated vinyl ester polymer (VE) with 1.25 weight % and 2.5 weight % exfoliated graphite nanoplatelates (1.25xGnP+VE and 2.5xGnP+VE respectively) in two different batches. One of the reinforced nanocomposite batches is toughened with 10 weight % almost unreactive liquid CTBN rubber (1.25xGnP+CTBN+VE and 2.5xGnP+CTBN+VE). The homogeneous exfoliation and dispersion is performed in 1 gal container for 4 hours, followed by 4 passes through a flow cell connected to a 100 W sonicator. The resin solution was mixed for 2 min with

FlackTek speed mixer at 3000 rpm. The solution of vinyl ester resin with xGnP and additional CTBN is poured into a mold, kept at room temperature for 30 minutes and then post cured at 80°C for 3 hours.

2.2. Dynamic direct tensile test set-up

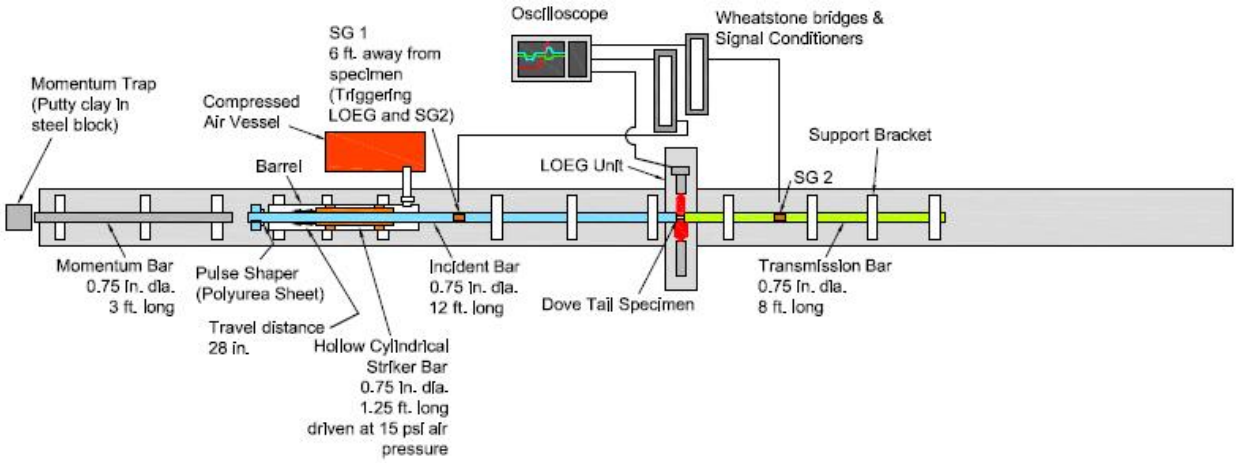

Figure 2.1: SHPB set-up for direct tensile tests including LOEG device.

The direct tensile SHPB system shown in Figure 2.1 is driven by a compressed air vessel connected with a solenoid switch valve to one end of a steel barrel having steel hollow cylindrical striker bar. The striker is mounted on two Teflon rings for achieving frictionless sliding motion inside the barrel. The striker bar is launched by air pressure, slides over the aluminum incident bar, inside the barrel and impacts the aluminum collar, mounted at the end of the incident bar, resulting in an incident tensile stress wave in incident bar. A thin ring-shaped polyurea pulse shaper is used at the impact-face of the collar for producing trapezoidal incident pulse. This collar, along with the incident bar, is retarded by a momentum bar which is trapped against a block of putty-clay. The specimen is mounted at other end of the incident bar is loaded with tensile stress and transmits the stress wave to the aluminum transmission bar.

Two sets of strain gages were attached at a distance away from the specimen on the incident and transmitted bars allowing the strain gages to capture the initiation of the incident, reflected and transmitted pulses distinctly. Each set consists of two gages located diametrically opposite side of the bar and connected in series (Figure 2.1). This arrangement compensates the bending effect of the bars and ensures uniaxial strain measurement. A digital oscilloscope connected to strain gages, through a Wheatstone bridge and signal conditioner, records the signal potential-time history during the test event. Strain pulse response in SHPB bars at the strain gage locations is applied in 1-D wave equation for estimating the tensile stress experienced by the test specimen.

2.2.1. Optimization of specimen geometry

A dog-bone shaped specimen and dovetail gripping mechanism [11] shown in Figure 2.2-a was adopted to reduce the wave dispersion, which can occur due to complex specimen attachment configurations of previously attempted pinned [3], threaded [8], or cementing [12] fixtures. A plane stress finite element analysis is carried out to optimize a specific shape that can prevent pre-mature failure of the specimen or the fixture due to undesirable stress concentrations, and also ensure uniform stress distribution within the gage section.

The length of specimen gage section is decided based on the dynamic pulse duration through the specimen. The pulse-wave needs to reverberate more than three times before failure initiation to ensure dynamic stress equilibrium in the specimen. The pulse speed in the specimen is predicted based on quasi-static properties previously obtained [32] according to ASTM 638-08 standard using typical dog-bone shaped specimen geometry [31].

The finite element model used for this purpose consists of two parts, the dog-bone shaped specimen and the dove-tail end fixture. Figure 2.2-b shows the load and boundary condition used in this model. The geometry is modeled using ANSYS Mechanical APDL® graphics tool and merged together as an assembly (Figure 2.2-c). The models are meshed with 10-noded elements

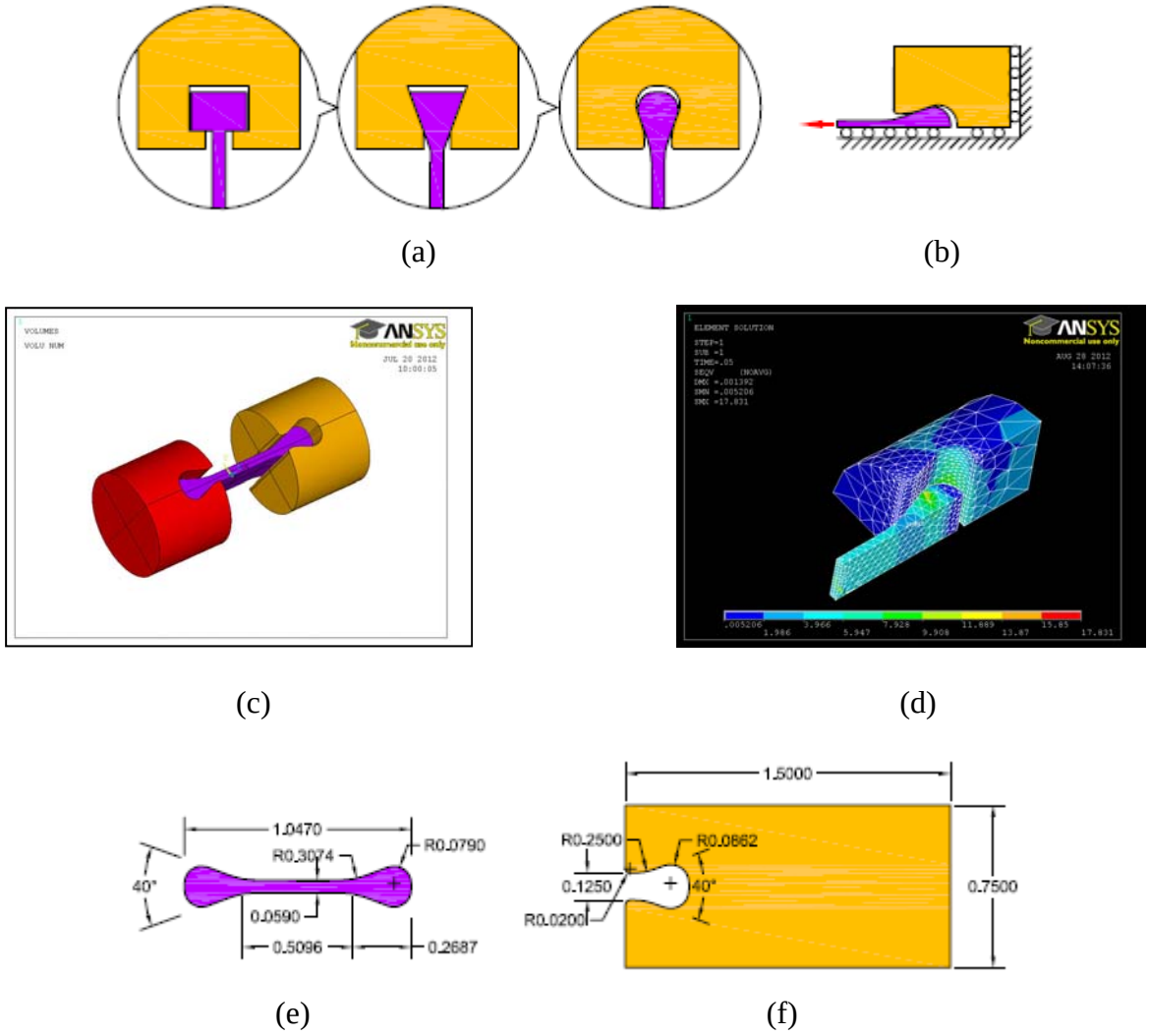

Figure 2.2: (a) Development of direct tensile specimen geometry, (b) boundary condition applied in stress analysis of specimen and fixture assembly, (c) ANSYS model, (d) von-Mises stress distribution in ANSYS simulation, (e) specimen dimensions, and (f) fixture dimensions (all dimensions are in inches)

(SOLID187 in ANSYS®) with quadratic displacement behavior and suitable for modeling irregular meshes. Quarter symmetry of the configuration was exploited to reduce the size of the model. This allowed the use of a much denser mesh for improving the accuracy of results.

Contact elements are used along the interface between the fixture and specimen. The contact was formulated for both the angular surfaces at normal and tangential directions. The constitutive law for contact elements includes a linear stress–strain behavior in the direction normal to the surface. The aluminum fixture surface is chosen as the master surface. The friction between the aluminum grip and specimen end is also accounted for using a stiffness-penalty method. The end of the fixture is constrained from translation in the axial direction, and a uniformly distributed tensile load is applied on the end surface of the specimen as shown in Figure 2.2-b. The color-map of von Mises stress distribution for an imposed distributed-load is shown in Figure 2.2-d. The uniformity of von Mises stresses in the gage section of the specimen is observable and validates the optimization of the specimen (Figure 2.2-e) and fixture (Figure 2.2-f) geometry. Appropriate test specimens are machined based on this optimized configuration using carbide tipped tool in CNC machine.

2.2.2. Validation of specimen failure

A fundamental requirement for validation of the direct dynamic tensile test is that the specimen failure should occur within gage section [31]. A high-speed camera (IDT Y7-S3) has been used in this validation process. The dynamic event is captured for 1.415 msec with 45 image-frames at a frame rate of 31,800 fps with 4 μs exposure. It is observed that the specimen fails at multiple locations within gage section (Figure 2.3) about 100 μs after the specimen is

loaded, which validates the optimized specimen and fixture geometry for characterizing the tensile properties of these nano-reinforced materials under dynamic direct tensile loading.

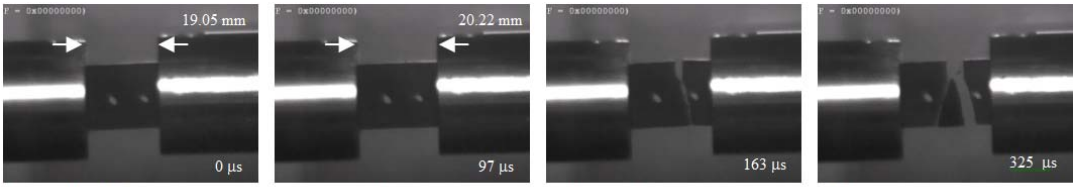

Figure 2.3: High-speed digital images of the specimen failure under high-strain rate direct tensile loading

2.2.3. Development of LOEG

A Laser Occluding Expansion Gage (Figure 2.4-a), incorporated for measuring the transverse tensile strain response, works on the principle of occluding a thin parallel laser sheet by either the specimen fixture ends (Figure 2.4-b-top) in case of direct dynamic tensile loading, or the deforming specimen geometry (Figure 2.4-b-bottom) in case of indirect dynamic tensile loading. This concept is adopted from the work of Ramesh and Narsimhan [49] on measuring radial strains in compression Kolsky bar experiment and later work of Chen et al. [50] on dynamic tensile response of low strength brittle solids.

The LOEG consists of a 635 nm wave-length laser system (© Coherent, Inc.) including single line projection head with 30° fan angle; two anti-reflector (MgF_2) coated plano-convex cylindrical N-BK7 glass lenses of 25 mm diameter with 50 mm focal length (© Edmund Optics); an amplified, switchable-gain, silicon PIN photo-detector with 1.5 MHz bandwidth at 4.25 GS/s sampling rate (© Thorlabs), and 0.2 mV noise level, and 100 MHz, 4 channel oscilloscope with 1.25 GS/s sampling rate (© Tektronix, Inc.). It is to be noted that the same oscilloscope used in

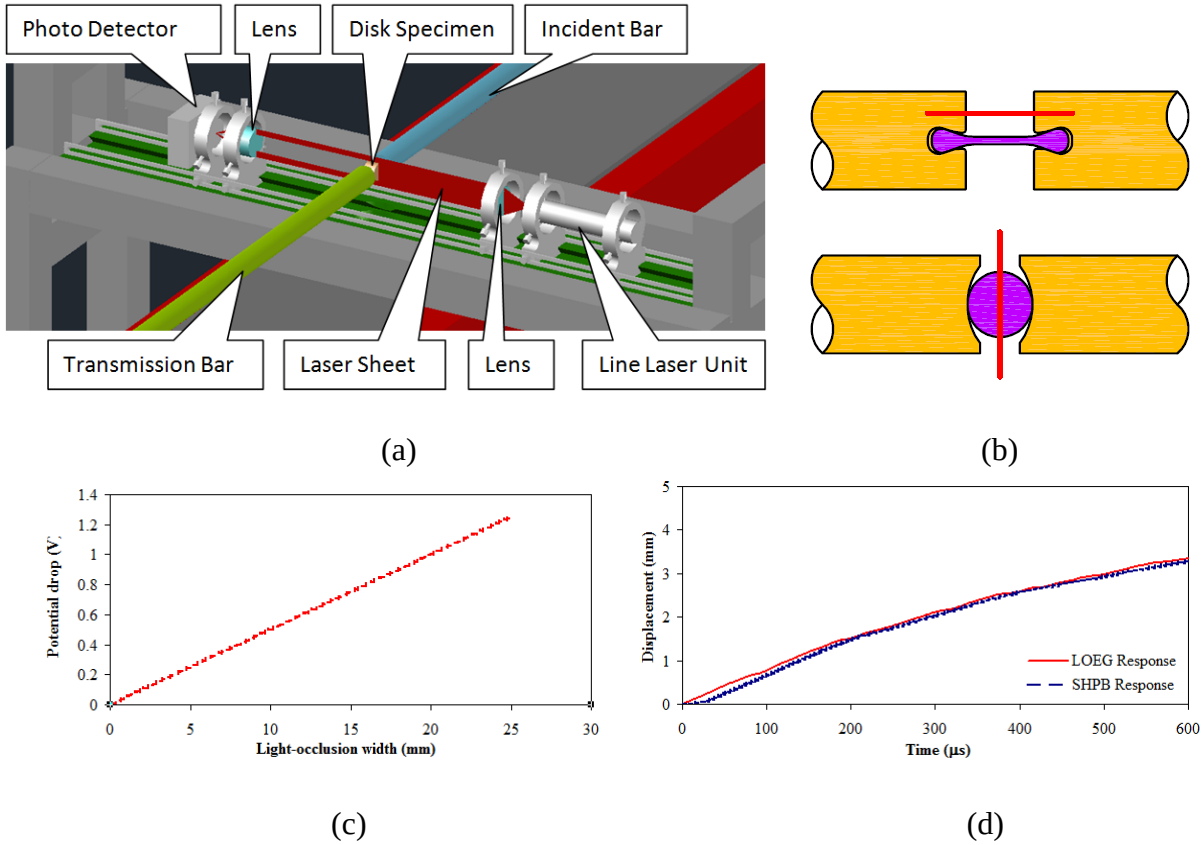

Figure 2.4: (a) LOEG test set-up, (b) line-projection (red line) of laser sheet in case of direct (top figure) and indirect (bottom figure) tensile tests, (c) static calibration of LOEG, (d) validation of LOEG calibration with SHPB application (comparing incident bar-end displacement estimated using SHPB strain gage response and the corresponding LOEG response)

SHPB system and the photo-detector is triggered by the incident pulse sensed at strain-gages mounted on the incident bar. The diode laser unit generates 635 nm laser beam collimated (converted from a divergent beam to a parallel beam over a long range of projection distance) with an elliptical cross-section of 3.8 mm × 0.9 mm. It consists of a single line projection head with 30° fan angle (angular spread of the laser beam). The projection head consists of Powell® glass lens which spreads the collimated laser beam and converts the elliptical projection into a 0.9 mm thick non-Gaussian line projection with almost uniform relative intensity along fan angle.

Line thickness is reduced to about 55 μm by pre-focusing collimated laser beam at target position of the specimen. The maximum power output is 5 mW. Black anodized aluminum housing holds the entire laser unit. The plano-convex cylindrical lens, made from coated N-BK7 glass substrate is used to achieve a parallel laser sheet of 25 mm (~ 1 inch) width. The high performance anti-reflection (MgF_2) coating has an average reflectance of less than 1.75% (per surface) in the wave length range of 400 - 700 nm. The light detection part consists of another similar plano-convex cylindrical lens arranged in symmetrically opposite orientation to converge the parallel sheet of light into a 9.8 mm diameter aperture of a photodiode light detector which is placed near the focal point of the laser sheet. The photodiode detector output is pre-amplified, and the opto-electronics and the preamplifier together have a bandwidth of 1.5 MHz. The output voltage of the detector is proportional to the total amount of laser light collected by the photo-detector. The whole system has a noise level less than 1 mV.

2.2.4. Calibration of LOEG

A precision micrometer gauge is used to partly occlude the laser sheet of 25 mm width with corresponding full field voltage output V. The occlusion ranges from 0 to 25 mm at a step of 0.1 mm. The corresponding photo-detector output (V_1) due to a specific displacement of the micrometer anvil is recorded. The displacement of the micrometer anvil (Figure 2.4-c) corresponds to a light-occlusion width (Δd) and certain amount of potential change ($V \sim V_1$).

Dynamic calibration is carried out with the same SHPB system. The collar mounted at end of the incident bar is impacted with the hollow striker bar and the motion of the other end of the incident bar was monitored using LOEG. When the tensile wave arrives at the free end of the incident bar, it is reflected as a compressive wave. The incident and reflected strain signals

measured from the strain gauge mounted on the incident bar. The strain signals are shifted on the travel time from the gauge position to the free end of bar. Then the displacement of the free end follows as [2]:

$$\Delta d = C\int_0^t (\varepsilon_i - \varepsilon_r)dt \tag{2.1}$$

where C is wave velocity in the incident bar, t is time of event and ε_i , ε_r are incident and reflected strain signals. With the LOEG output, the displacement of the free end of the incident bar is calculated using calibrated LOEG response for comparing the values obtained with equation 5. The comparison (Figure 2.4-d) of the calibrated LOEG response with the response obtained from strain gages mounted on incident bars shows excellent agreement, and demonstrates that the LOEG has sufficient bandwidth for valid measurements in SHPB testing.

2.2.5. Stress measurement

The incident pulse propagates along the incident bar before it pulls the sample, developing in the reflected and transmitted stress waves. In this test, the steel hollow-cylindrical striker bar impacts aluminum collar mounted at the end of aluminum incident bar. Due to the striker-collar impedance mismatch, the incident pulse exhibits a long unloading portion with progressively decreasing amplitudes similar as described in [51]. Hence, the initial maximum amplitude portion of the incident pulse is used for SHPB analysis. The candidate materials having low-impedance and low-dynamic tensile strength allow only a small portion of the loading pulse to be transmitted into the transmission bar. Since, the transmitted pulse is too weak to estimate stress, an alternative one-dimensional wave propagation analysis [52] is considered for estimating direct tensile stress (σ_{dt}) as shown in the following equation -

$$\sigma_{dt} = \frac{2A_s\rho_s C_s}{A_i\rho_i C_i + A_s\rho_s C_s}.\frac{A_i}{A_s}.E_i\varepsilon_i \qquad (2.2)$$

where E is elastic modulus; ε denotes the strain; A, ρ and C are cross-sectional area, density and wave velocity for the incident bar and the specimen. The subscripts i and s indicate the incident bar and the specimen respectively.

2.2.6. Strain measurement

The laser sheet, projected horizontally above the direct tensile test-specimen, is partially occluded by the ends of the specimen fixtures mounted on incident and transmission bars. In our

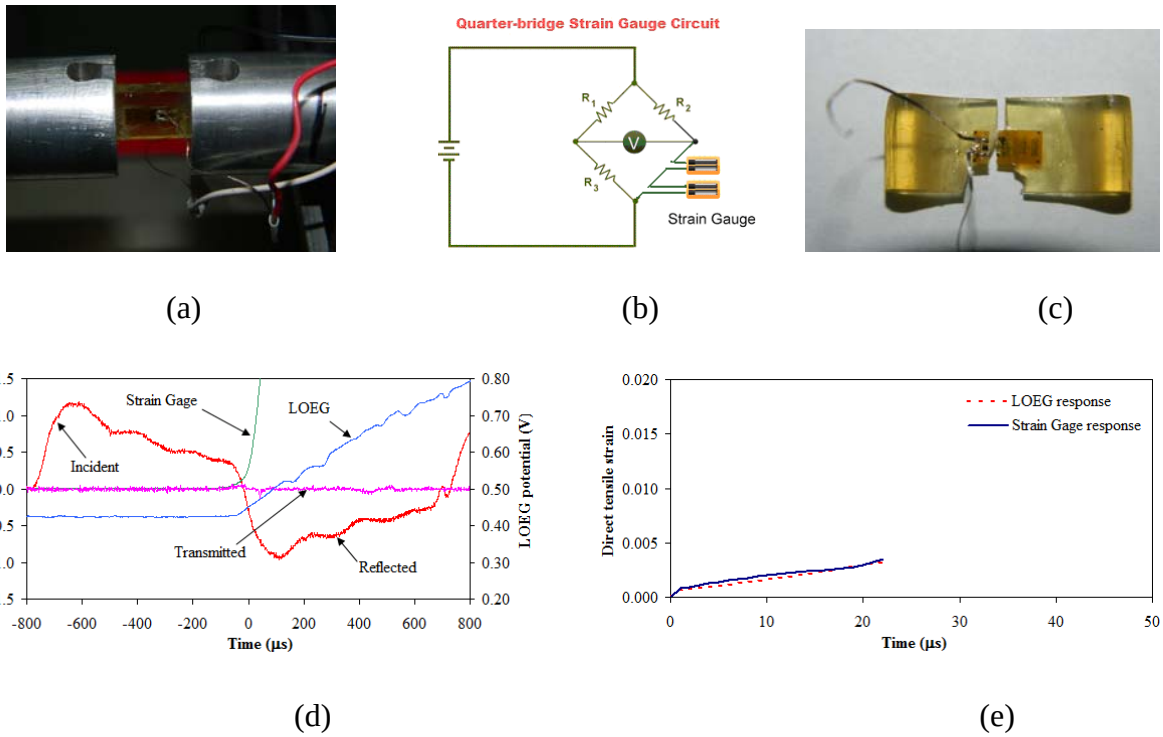

Figure 2.5: High-strain rate direct tensile tests (a) optimized specimen mounted in SHPB, (b) Wheatstone bridge circuit diagram, (c) post-test specimen including strain gage, (d) simultaneous LOEG and strain gage response from SHPB test, and (e) the direct tensile strain history obtained from LOEG and strain gage responses

experimental set-up, gap between specimen fixture holding ends is almost equivalent to the specimen gage length. Hence, the required tensile strain is directly estimated from the ratio of the increment of potential (ΔV) during specimen elongation to the initial potential (V) due to the placement of the specimen in the fixtures mounted at the end of incident and transmission bars.

A comparative study of the LOEG response is performed by installing strain gages on the dog-bone shaped specimen and obtaining the direct tensile strain simultaneously using both LOEG and on-specimen strain gages (Figure 2.5-a). Two strain gages are mounted on opposite sides (Figure 2.5-a) of the specimen and connected in quarter bridge circuit (Figure 2.5-b) through a digital strain indicator system. Figure 2.5-c shows a typical post-test failed specimen including strain gage. The dynamic response was plotted as the direct tensile strain-time history of the specimen. Simultaneously LOEG provided comparative strain response to the same oscilloscope (Figure 2.5-d). Obtaining almost similar strain-time history from both strain-gage and LOEG (Figure 2.5-e), validates application of LOEG for the direct tensile measurements.

2.3. Dynamic indirect tensile test set-up

Experimental facilities used in this study consist of a traditional compression split-Hopkinson pressure bar system that has been modified to conduct indirect dynamic tensile tests on nanocomposite specimens based on conventional Brazilian disk test method.

2.3.1. Adaptation of SHPB test system

Experimental facilities used in this study consist of a traditional compression split-Hopkinson pressure bar system that has been modified to conduct indirect dynamic tensile tests on nanocomposite specimens based on conventional Brazilian disk test method. The SHPB

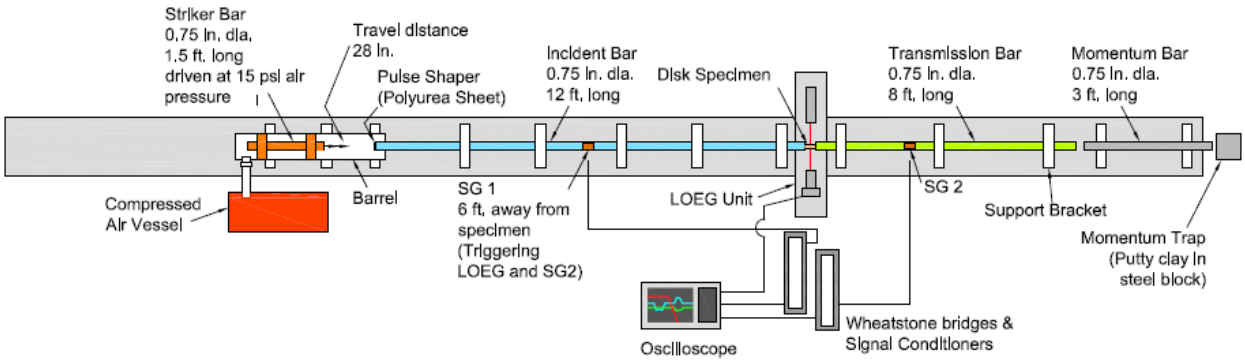

Figure 2.6: SHPB setup for indirect tensile tests including Laser Occluding Expansion Gage (LOEG) system

system (Figure 2.6) is driven by a compressed air vessel of 1.2 MPa (175 psi) capacity connected with a solenoid switch valve to one end of the 38 mm (1.5 inch) inside diameter and 1.2 m (4 ft.) long steel barrel having convex-end solid cylindrical striker of 0.457 m (1.5 ft.) long. The striker is mounted on two Teflon rings for achieving frictionless sliding motion inside the cylinder. The overall system consists of an incident bar of 3.7 m (12 ft.) long, a transmission bar 2.4 m (8 ft.) long, momentum bar 0.9 m (3 ft.) long and a momentum-trap made of white putty clay packed in a robust steel frame. The bars and the striker were made from 19 mm diameter (0.75 inch) Aluminum (Al 6061-T6) bars with elastic modulus of 68.9 GPa, density of 2700 kg/m^3 and nominal yield strength of 276 MPa [53]. The complete arrangement is mounted on a 30 ft. long, 2 ft. height and 0.5 ft. wide I-beam horizontally leveled on concrete floor.

Two sets of 350 Ω strain gages (CEA-06-250UW-350) from Vishay Micro-measurement Group were attached at a distance away from the specimen on the incident and transmitted bars allowing the strain gages to capture the initiation of the incident, reflected and transmitted pulses distinctly. Each set consists of two gages located diametrically opposite side of the bar and connected in series (Figure 2.6). This arrangement compensates the bending effect of the bars

and ensures only axial strain measurement. A digital oscilloscope of model TDS 3014C from Tektronix is connected to strain gages, through a Wheatstone bridge and a signal conditioner (Model 2310B from Vishay Micro-measurement), records the signal potential-time history during the test event. The strain pulse response in SHPB bars at strain gage locations is obtained by multiplying a conversion factor which is a function of bridge excitation, amplifier gain and gage factor of strain gage. Negative magnitude is considered in case of compressive pulse.

2.3.2. Adaptation of Brazilian disk test system

The Brazilian disk test method [45] is an indirect approach for obtaining the tensile strength of high-stiffness low-strength brittle materials. It assumes a state of plane stress in the disk due to the application of diametrically opposite loading on the disk specimen [45, 46]. The tensile stress [45-46] induced at the center of the specimen along the transverse diameter of the disk specimen has been analytically and experimentally determined as $2P/(\pi DL)$, where, P is the applied compressive load, D is the diameter of the specimen, L is the specimen thickness.

Conventional Brazilian disk method proposes flat-end anvils for loading the circular disk specimen. The disadvantage of this approach is a large stress concentration at the lines along the thickness of the specimen. Hence, in most of the cases immature failure occurs close to the loading lines [54]. Two controlled loading approaches have been tried in this investigation. The geometry of the disk specimen was modified in the first attempt. The diametrically opposite loading lines along the thickness of the specimen were made flat [55] for about 20° angle subtended at the center of the specimen to decentralize the stress concentration at the loading point and hence the relation of induced tensile stress with applied compressive load was modified based on the subtended angle by the flat-ends. The disadvantage of this approach is that

the specimens rupture at the edges of the flat-ends, instead of at the center of the specimen. It is observed that the flatness and parallelity of the flat ends are crucial for a successful test. High precision in specimen preparation is required and achieving that level of geometric accuracy is practically difficult in case of quasi-brittle materials.

The second approach eliminates all these complexities by modifying the flat-end of anvil to circular concave ends [54]. Also the concave ends hold the disk specimen more securely than flat-ends in horizontal SHPB testing. The stress concentration is optimally reduced with failure

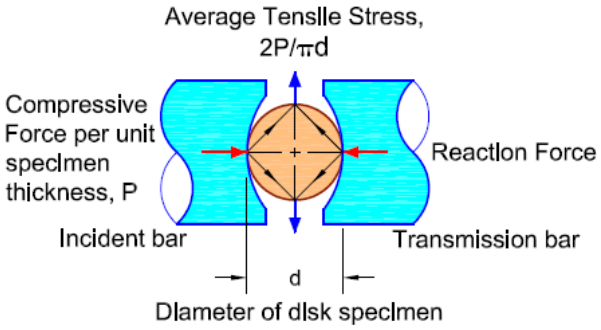

Figure 2.7: Induced tensile stress in circular disk specimen along transverse direction due to applied compressive loading

of the disk specimen initiating at the disk-center and propagating along the compressive loading axis, thus ensuring a valid indirect tensile test (Figure 2.7).

The incident and transmission bars are threaded and coupled with respective concave end fixtures. The disk specimen is diametrically held in between the larger diameter concaved surfaces of the loading fixtures.

A pulse shaper is employed to achieve dynamic force balance in the specimen during the experiment. The pulse shaping technique is discussed in detail by Frew et al. [48] for SHPB

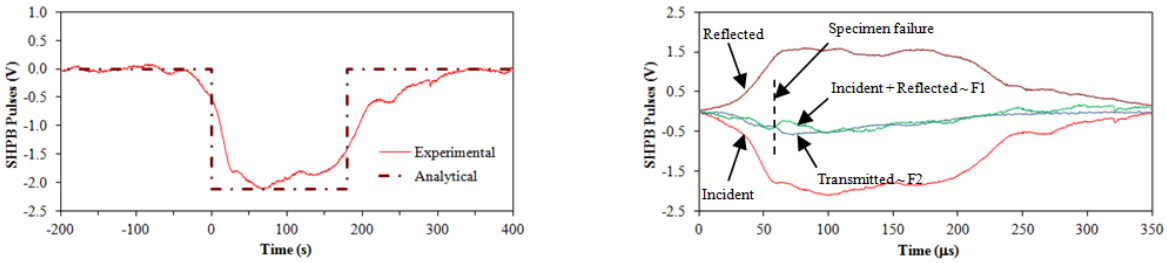

(a) (b)

Figure 2.8: (a) Typical incident pulse applied in high strain rate indirect tensile test, (b) dynamic force balance during a typical high-strain rate indirect tensile test

compressive tests of brittle materials. In a traditional SHPB test, the incident wave with rectangular stress-pulse may initiate undesired damage to the specimen upon impact before achieving stress equilibrium. If forces on both sides of the specimen are not the same during test event, the test can not be considered as valid [56]. A polyurea disk, 0.313 inch in diameter and 0.003 inch in thickness, is used for shaping the incident wave from a rectangular to a trapezoidal wave (Figure 2.8-a). This rubbery pulse shaper ramps the incident pulse such that the tensile stresses induced in the disk specimen can achieve an equilibrium state before diametrical splitting of the specimen occurs. Figure 2.8-b shows the pulses on both ends of the specimen in a typical test. The dynamic force (F_1) on the end of the specimen towards incident bar is proportional to the sum of the incident and reflected stress waves, and the dynamic force (F_2) on the other end of the specimen towards transmission bar is proportional to the transmitted stress wave. It can be seen from Figure 2.8-b that the dynamic pulses responsible for these two forces on both sides of the specimen remain almost identical during the whole dynamic loading period. The inertial effects are thus eliminated because of the absence of global force difference in the specimen and the static equilibrium analysis can be applicable [47].

2.3.3. Validation of test set-up

The fundamental requirement for the validation of the Brazilian disk test method is that the initiation of specimen failure should occur at the center of the specimen and propagate through the diameter along the compressive loading axis [45]. At high strain rate loading, the failure occurs within micro- to milli-second depending on the brittleness of the material. Human eye is able to persistently and distinguishably observe only such dynamic events which occur in more than 40 mili-seconds [57] apart and thus cannot record this phenomenon; hence a high-speed camera is essential in this validation process. The SHPB operating air pressure is maintained at 10 psi and a specimen of 19 mm (0.75 inch) diameter was tested to ensure the recording of the diametrical fracture phenomena according to the capability of the high-speed camera (Hadland HPV-2 Shimadzu), used in this observation. The resolution of the images is compromised due to increased frame rate of 250,000 fps. The dynamic event is captured for 408 μs with 102 image-frames with 1 μs exposure. It is observed that the specimen expands along the diameter, orthogonal to the loading axis and the failure occurs through the diameter along the compressive loading axis (Figure 2.9) within 48 to 52 μs. The fracture is initiated at the center of

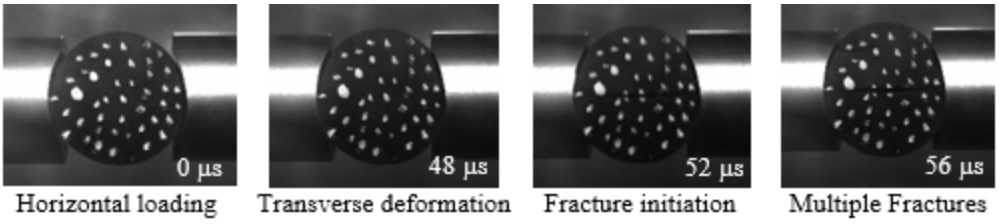

Figure 2.9: High-speed digital images of the specimen failure due to transverse tensile stress induced by high-strain rate diametric compressive loading (white spots on specimens are for performing 2D-DIC in image processing software for further analysis)

the specimen and propagates through the diameter along the loading axis towards the points of loading. The maximum expansion occurs along transverse diameter of the specimen, which validates this experimental setup for characterizing the tensile properties of the materials under compressive diametrical loading.

2.3.4. Disk-specimen preparation

Nanocomposite disk specimens with a diameter of 12.7 mm (0.5 inch) are machined using carbide tipped tool in CNC machine from molded panels with thickness of 10 mm (0.4 inch). The diameter of specimen is decided based on the dynamic pulse duration through the diameter of the specimen. The pulse-wave needs to reverberate more than three times before failure initiation to ensure dynamic stress equilibrium in the specimen. The pulse speed in the specimen is predicted based on quasi-static properties (Table 1.1) obtained [32] according to ASTM 638-08 [31] using the typical dog-bone specimen geometry. For ensuring uniform test-load distribution along the specimen thickness, the roundness and cylindricity error of the disk specimen are kept to a minimum.

2.3.5. Stress measurement

In dynamic indirect tensile test initiates failure of the disk specimen at the disk-center and propagates along the compressive loading axis (Figure 2.10-a), thus ensuring a valid indirect tensile test. Figure 2.10-b shows the typical SHPB and LOEG response of vinyl ester nanocomposites subjected to indirect tensile load at high-strain rate. The forces on the two ends of the specimen along the SHPB loading axis are estimated as [55]:

$$P_1 = AE\left(\varepsilon_i + \varepsilon_r\right) \text{ and } P_2 = AE\varepsilon_t \tag{2.3}$$

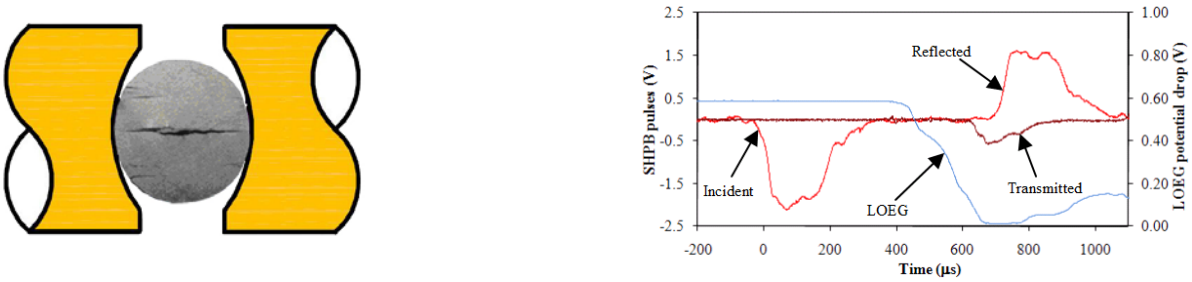

(a) (b)

Figure 2.10: (a) Splitting of disk specimen under induced indirect tensile stress, (b) typical SHPB and LOEG response of vinyl ester nanocomposites from high strain rate indirect tensile test

where E is elastic modulus of the bar material, A is the cross-sectional area of the bar, ε denotes strain and subscripts i, r indicates incident and reflected pulses. Average of these two forces is considered as the applied diametric compressive load, P.

The Brazilian disk test method assumes a state of plane stress in the disk-specimen due to application of diametrically opposite loading [45-47]. The in-plane stresses along the transverse diameter AB (Figure. 2.11-a) of the disk specimen obeys the following equations [47, 52] -

$$\sigma_x = \frac{2P}{\pi DL}\left[1-\left\{\frac{D\cos^3\theta}{r}+\frac{D(D-r\cos\theta)^3}{\left(r^2+D^2-2Dr\cos\theta\right)^2}\right\}\right]=\frac{2P}{\pi DL}\left\{1-\frac{4D^4}{\left(4y^2+D^2\right)^2}\right\} \tag{2.4}$$

$$\sigma_y = \frac{2P}{\pi DL}\left[1-\left\{\frac{D\cos\theta\sin^2\theta}{r}+\frac{D(D-r\cos\theta)r^2\sin^2\theta}{\left(r^2+D^2-2Dr\cos\theta\right)^2}\right\}\right]=\frac{2P}{\pi DL}\left\{1-\frac{16D^2y^2}{\left(4y^2+D^2\right)^2}\right\} \tag{2.5}$$

$$\tau_{xy}=0 \tag{2.6}$$

where, P is the applied compressive load, D is specimen diameter, L is specimen thickness and 'y' is co-ordinate along the specimen's transverse diameter. The tensile stress (σ_t) induced at the specimen center is obtained from equation (4) as $2P/(\pi DL)$.

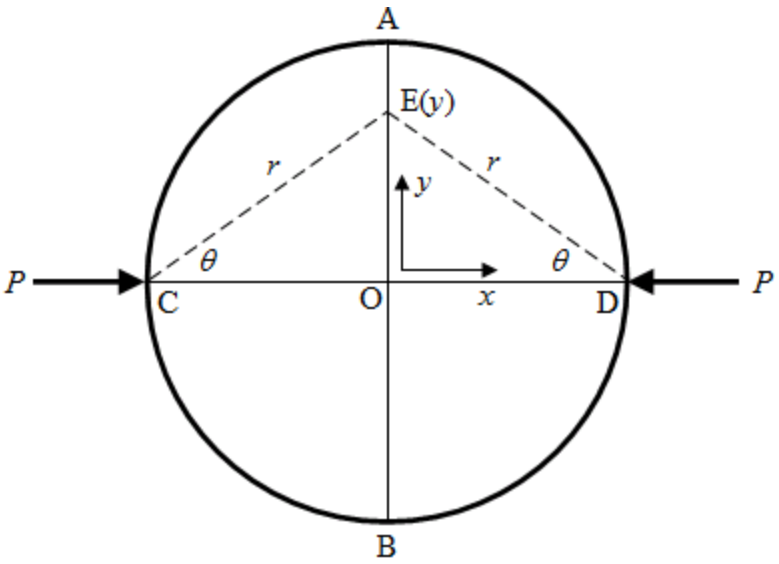

(a)

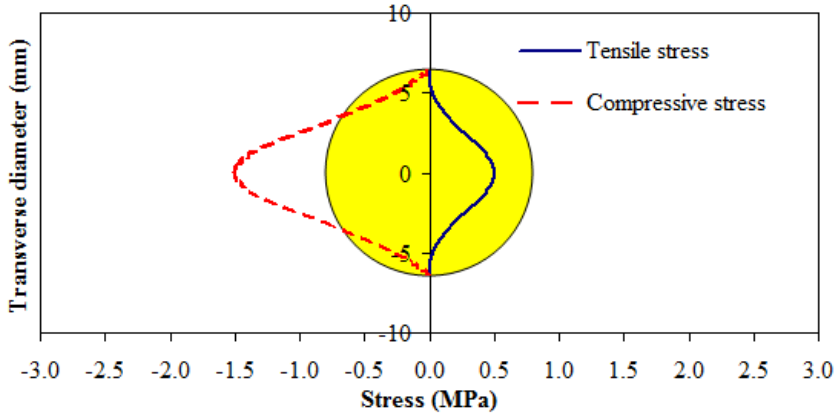

(b)

Figure. 2.11: (a) Brazilian disk subjected to diametrical compressive load, *P*, (b) stress distribution along vertical diameter of Brazilian disk subjected to compressive load along the horizontal diameter

The analytically obtained stress distribution along the transverse diameter AB (shown in Figure. 2.11-b) indicates that the center of the disk experiences about 3 times larger compressive stress of $6P/(\pi DL)$ as derived from equation (2.4), than the indirect tensile stress of $2P/(\pi DL)$ obtained from equation (2.5). The effect of this compressive stress on indirect tensile stress

cannot be ignored for obtaining the actual indirect tensile strain. As such, the actual tensile strain-time history cannot be obtained by measurements made from this indirect test method but can be corrected analytically, as discussed in the following section.

2.3.2. Strain measurement

Strain measurement is crucial in case of adapting Brazilian disk test method. The corresponding strain over the disk diameter AB can be analytically estimated by the following equation [58] -

$$\varepsilon_{AB} = \frac{1}{2L_g E_t}\int_{-Lg}^{Lg}\left(\sigma_y - \nu\sigma_x\right)dx \tag{2.7}$$

where, E_t and ν are tensile modulus and Poisson's ratio of the specimen, L_g is half of gage length along AB. Substituting equations (2.4) and (2.5) in equation (2.7) and solving the integral, the analytical expression for the strain measured in Brazilian test is obtained from the following equation -

$$\varepsilon_{AB} = \frac{2P}{\pi DLE_t}\left\{\left(1-\frac{D}{L_g}\tan^{-1}\frac{2L_g}{D}\right)(1-\nu)+\frac{2D^2(1+\nu)}{4L_g^2+D^2}\right\} = \varepsilon_t.F_c \tag{2.8}$$

$$\text{where, } F_c = \left(1-\frac{D}{L_g}\tan^{-1}\frac{2L_g}{D}\right)(1-\nu)+\frac{2D^2(1+\nu)}{4L_g^2+D^2} \tag{2.9}$$

F_c is the correction factor required for estimating the actual tensile strain (ε_t) history from a Brazilian disk test. It is obvious from equation (2.8) or (2.9) that the actual tensile strain response from the Brazilian disk test method depends on the Poisson's ratio (ν), the gage length ($2L_g$) and the diameter (D) of the specimen. The size effect can be eliminated by considering specimen diameter (D) as the gage length ($2L_g$) which reduces equation (2.9) to the following:

$$F_c = 2\left(1 - \tan^{-1}1 + \nu \tan^{-1}1\right) = 0.43 + 1.57\nu \tag{2.10}$$

For the vinyl ester based nanocomposites, with Poisson's ratio ν = 0.36 - 0.37, the correction coefficient factor obtained from equation (2.10) is close to 1. As such, considering the diameter as effective gage length eliminates the analytical complexities for obtaining the actual tensile strain response with this indirect tensile test method. This may not be valid, however, for materials with Poisson's ratio beyond the range of 0.35 -0.40, where the correction coefficient factor should be considered appropriately from equation (2.10).

According to the non-Gaussian nature of intensity of the laser line-projection, the calibration factor is spatial along the projection length. Hence, an alternative approach has been adopted to avoid the dependency on the LOEG calibration factor in strain measurement. The full-field potential output due to non-occluded laser was recorded as the base-line potential for a measurement. Any occlusion of laser due to the presence and deformation of the specimen across the path of laser is reflected as the drop of potential. The required indirect tensile strain is estimated from the ratio of the increment of drop of potential (ΔV) during specimen deformation to the initial drop of potential (V) due to the placement of the specimen across the path of laser sheet. This approach eliminates the requirement of diameter measurements and consequently does not depend on a fixed calibration factor for the LOEG system.

A comparative study is performed by obtaining the indirect tensile strain simultaneously using the LOEG set-up and a strain gage (EA-06-062DN-350) installed on the disk specimen. The single strain gage is mounted on one side of the disk specimen (Figure 2.12-a) and connected in quarter bridge circuit (Figure 2.12-b). Figure 2.12-c shows typical specimen installation on SHPB along with on-specimen strain gage. The LOEG setup provided

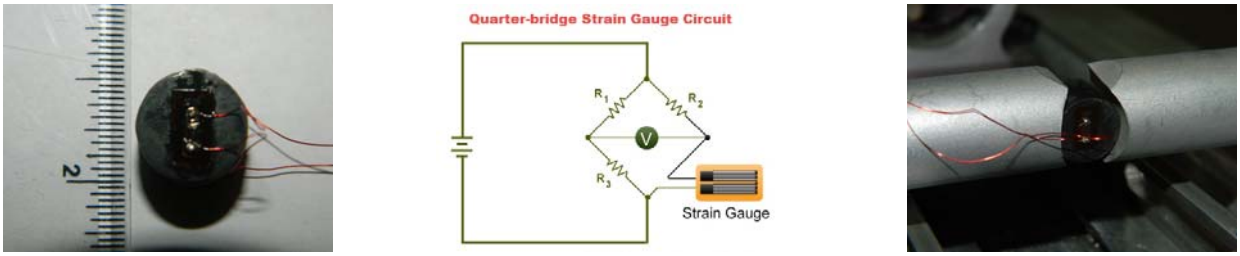

(a) (b) (c)

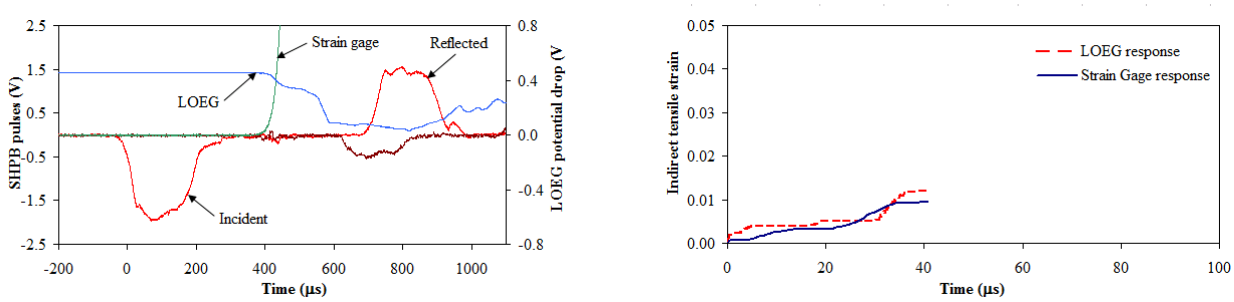

(d) (e)

Figure 2.12: High-strain rate indirect tensile tests (a) specimen with strain gage, (b) Wheatstone bridge circuit diagram, (c) specimen mounted in SHPB, (d) simultaneous LOEG and strain gage response from SHPB test, and (e) indirect tensile strain history obtained from LOEG and strain gage responses

simultaneous strain response along with on-site strain gage response to the same oscilloscope (Figure 2.12-d). This comparative investigation, obtaining a similar strain-time history from both the strain-gage and LOEG responses (Figure 2.12-e), validates the application of LOEG for indirect tensile strain measurement.

2.4. Quasi-static indirect tensile test set up

Quasi-static indirect tensile experiments are conducted on EnduraTec, a pneumatically driven materials test system (Figure 2.13-a) for evaluating the strain-rate effects over a broad

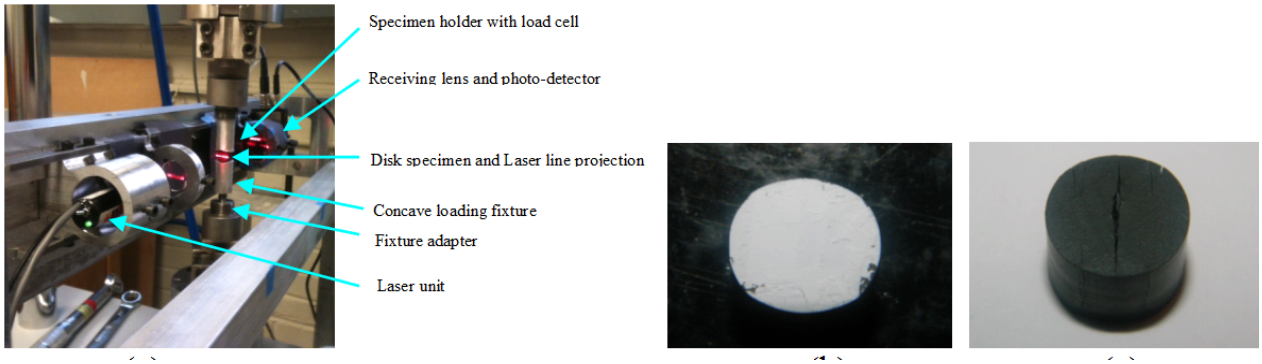

(a) (b) (c)

Figure 2.13: (a) Quasi-static indirect tensile test setup, (b) post-test pure vinyl ester sample deformed elliptically without splitting, (c) reinforced nanocomposite with diametrical splitting

range of loading. An interface load cell is used to measure the axial load. The disk specimen is mounted diametrically within the same concave end fixtures for obtaining identical boundary condition applied in SHPB tests. LOEG unit is oriented transversely with respect to the loading axis for measuring the induced transverse tensile strain in disk specimen. Pure vinyl ester sample deforms elliptically without splitting (Figure 2.13-b), whereas reinforced nanocomposite fails with diametrical splitting (Figure 2.13-c).

2.5. Dynamic compressive test set-up

A traditional compression SHPB set-up with aluminum bars is used for obtaining dynamic compressive response of the candidate materials. The same disk specimen geometry considered for indirect tensile tests is maintained, but loaded axially on the opposite faces under compression. The compressive 1-D wave propagating through the specimen thickness is considered for computing the dynamic compressive stress and strain histories.

CHAPTER III EXPERIMENTAL RESULTS AND DISCUSSION

Figure 3.1 shows the typical failure of an optimized dog-bone specimen under high-strain rate direct tensile loading in SHPB. The fact that more than one fracture surface exists, as shown in Figure 3.1, indicates that dynamic stress equilibrium is reached before fracture events take place. Figure 3.2-a shows a typical SHPB and LOEG response of high strain rate tensile test. Initiation of a crack in the specimen is indicated by the instantaneous drop (Figure 3.2-b) of stress. The corresponding time of the visible first stress peak (considered also as the dynamic direct tensile strength) has been taken as the time-instant of crack-initiation. The corresponding

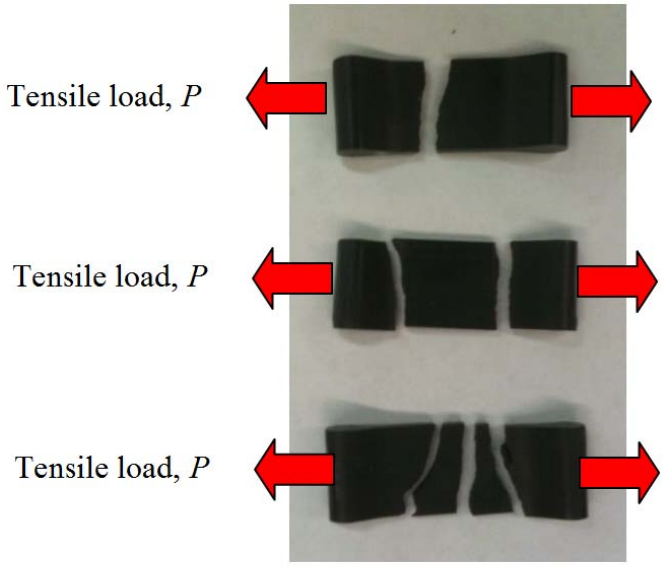

Figure 3.1: Typical failed specimens under high-strain rate direct tensile test (multiple fractures indicate stress uniformity along the specimen gauge length)

strain developed at that time-instant (Figure 3.2-c) is designated as the ultimate tensile strain of the specimen under dynamic direct tensile loading. The energy absorbing capacity (E), i.e, the energy necessary to deform a specimen per unit volume, is evaluated by integrating the area (Figure 3.2-d) under the stress vs. strain curve [59] as follows

$$E = \int_0^{\varepsilon_{ut}} \sigma_t(\varepsilon) d\varepsilon \tag{3}$$

where, σ_t is the induced tensile stress, ε is the corresponding transverse diametrical tensile strain and ε_{ut} is the ultimate strain.

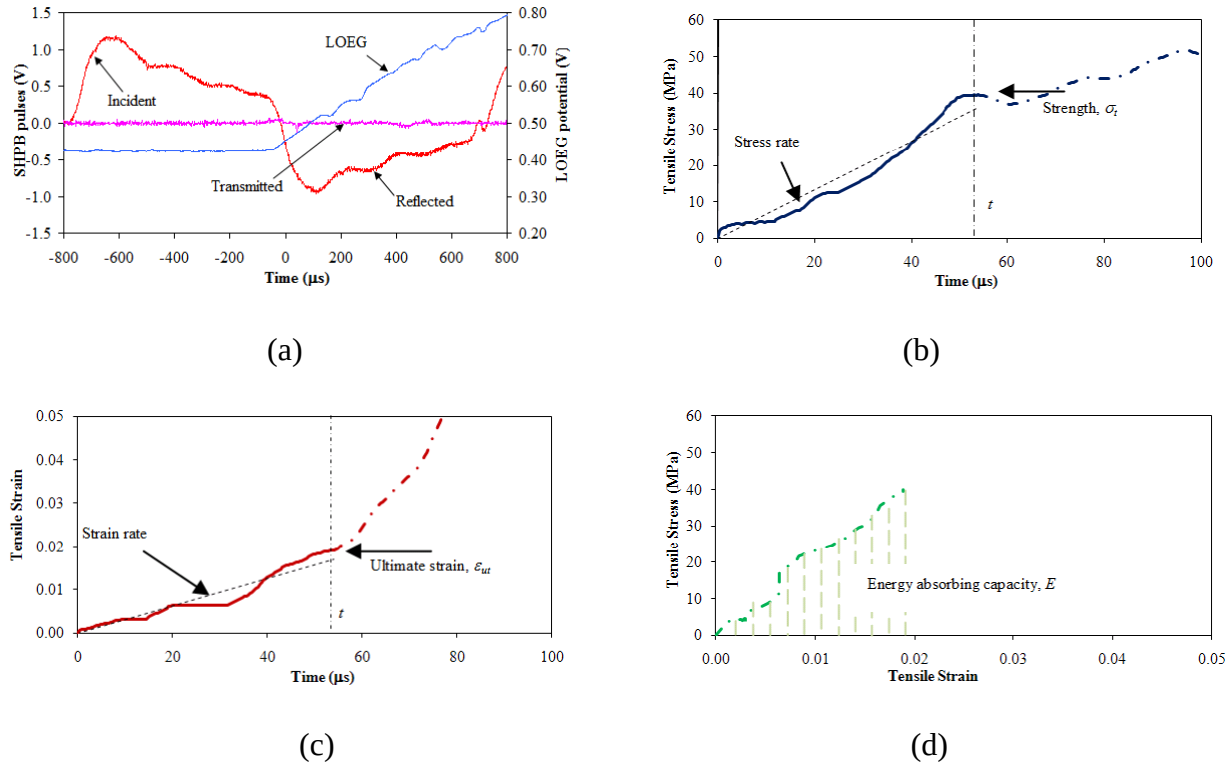

Figure 3.2: Typical SHPB and LOEG response of vinyl ester nanocomposites in high strain rate direct tensile test, (a) SHPB and LOEG response, (b) stress-time history (c) strain-time history, and (d) energy absorbing capacity estimation from stress-strain curve

3.1. Dynamic direct tensile response

Figure 3.3 summarizes the dynamic direct tensile response of xGnP reinforced and also with additional CTBN toughened vinyl ester nanocomposites, at a strain-rate of about 1000 s^{-1}

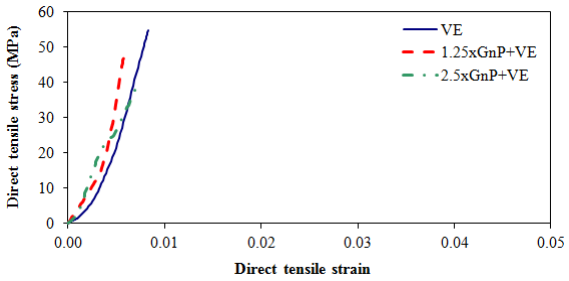

i. (a)

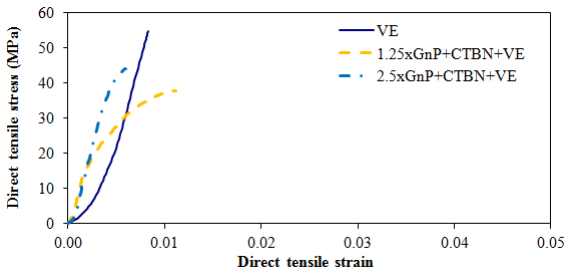

i. (b)

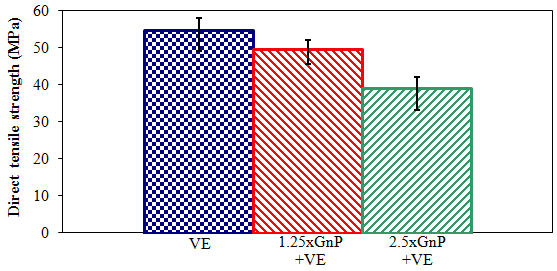

ii. (a)

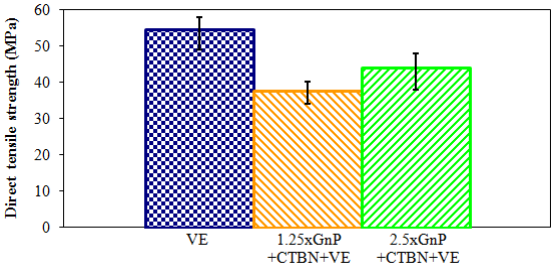

ii. (b)

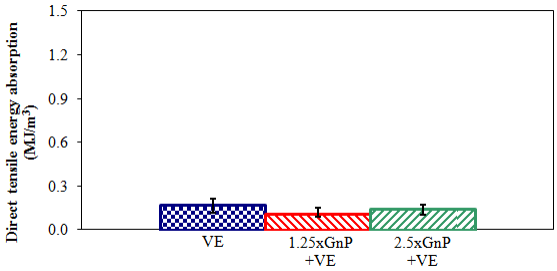

iii. (a)

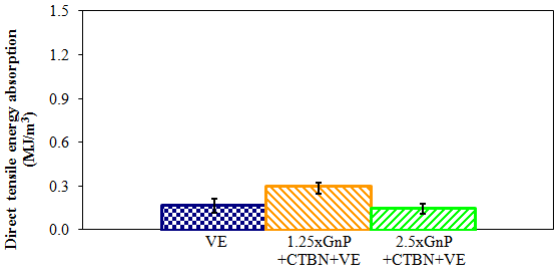

iii. (b)

Figure 3.3: High-strain rate direct tensile response from SHPB tests (i) typical stress vs. strain behavior, (ii) strength, and (iii) energy absorbing capacity of (a) graphite platelet reinforced, and (b) with additional CTBN toughened vinyl ester nanocomposites

from SHPB tests. All the nanoreinforced specimens including pure vinyl ester failed in a brittle manner under dynamic tensile loading (Figure 3.3-i). It can be observed that the tensile strength of pure vinyl ester decreases marginally with xGnP reinforcement (Figure 3.3-ii-a). Addition of CTBN toughening to xGnP reinforced nanocomposites did not show significant improvement (Figure 3.3-ii-b). Energy absorbing capacity of pure vinyl ester has remained almost the same with xGnP (Fig. 10-iii-a) reinforcement. However, this is marginally improved by further CTBN toughening to the xGnP reinforced nanocomposites (Figure 3.3-iii-b).

3.2. Dynamic indirect tensile response

Indirect tensile response of xGnP reinforced and with additional CTBN toughened vinyl ester nanocomposites at strain-rate of about 1000 s^{-1} from SHPB tests is illustrated in Figure 3.4. All the candidate material samples fail without yield under dynamic tensile loading (Figure 3.4-i). It can be observed that the tensile strength of pure vinyl ester remains unchanged with xGnP reinforcement (Figure 3.4-ii-a). Addition of CTBN toughening to the 1.25 wt.% xGnP reinforced nanocomposites shows a marginal improvement (Figure 3.4-ii-b). The energy absorbing capacity of pure vinyl ester is improved with xGnP (Figure 3.4-iii-a) reinforcement. However, this improvement is reduced about 50% by further CTBN toughening to the xGnP reinforced nanocomposites (Figure 3.4-iii-b).

Comparative investigation of the dynamic direct and indirect tensile responses shows similarity, to some extent. Energy absorbing capacity of the reinforced candidate materials is observed to be distinctively more in indirect tensile response (Figure 3.4-iii-a) than the direct tensile response (Figure 3.3-iii-a). These observed discrepancies of responses from two different approaches appear to be due to the heterogeneity of the candidate materials and perhaps the

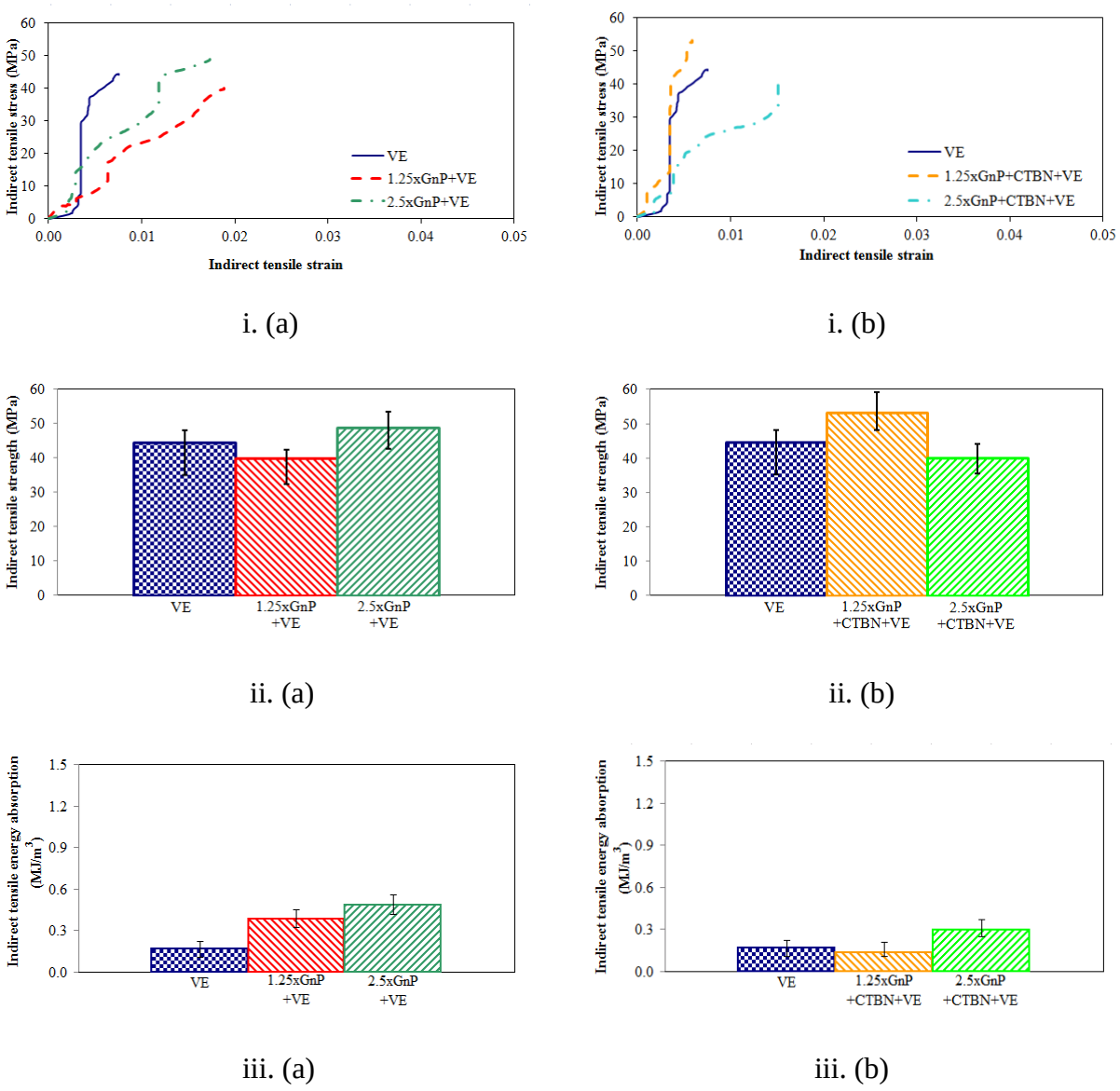

Figure 3.4: High-strain rate indirect tensile response from SHPB tests (i) typical stress vs. strain behavior, (ii) strength, and (iii) energy absorbing capacity of; (a) graphite platelet reinforced, and (b) with additional CTBN toughened vinyl ester nanocomposites

effect of specimen size. In direct tensile test, due to the striker-collar impedance mismatch, the incident pulse exhibits a long unloading portion with progressively decreasing amplitudes, and hence, the initial maximum amplitude portion of the incident pulse is used for SHPB data analysis. Due to the weak pulse transmission in dynamic direct tensile tests, an alternative

approach is considered for estimating stress. This approach mostly depends on quasi-static properties of the candidate materials; hence the stress-time history obtained in this test method could be questionable. It is possible to increase the transmitted pulse signal, if the impedance and/or cross-sectional area of the transmission bar is reduced significantly.

3.3. Quasi-static indirect tensile response

The quasi-static (0.015 mm/s displacement controlled at 0.001 s^{-1} strain rate) indirect tensile response shows a detrimental effect of the inclusion of xGnP and CTBN to pristine vinyl ester (Table 3.1). The pure vinyl ester specimens (Figure 2.13-b) showed ductile deformation response beyond the load cell limit (10 kN). Hence, the conventional Brazilian disk test method, which is more appropriate for brittle materials, could not capture the true behavior of pure vinyl ester under quasi-static loading due to its ductility. It is, therefore, recognized that the modulus,

Table 3.1: Quasi-static indirect tensile properties of nanocomposites obtained from Brazilian disk test method

Matrix	**Reinforcement**	**Toughening agent**	**Elastic Modulus (GPa)**	**Strength (MPa)**	**Ultimate strain (%)**
Brominated Vinyl ester	None	None	1.29	35.9	3.38
Brominated Vinyl ester	1.25 wt.% xGnP	None	3.93	26.8	1.50
Brominated Vinyl ester	2.5 wt.% xGnP	None	3.73	29.8	0.98
Brominated Vinyl ester	1.25 wt.% xGnP	10 wt.% CTBN	4.49	29.1	2.13
Brominated Vinyl ester	2.5 wt.% xGnP	10 wt.% CTBN	5.14	27.6	1.34

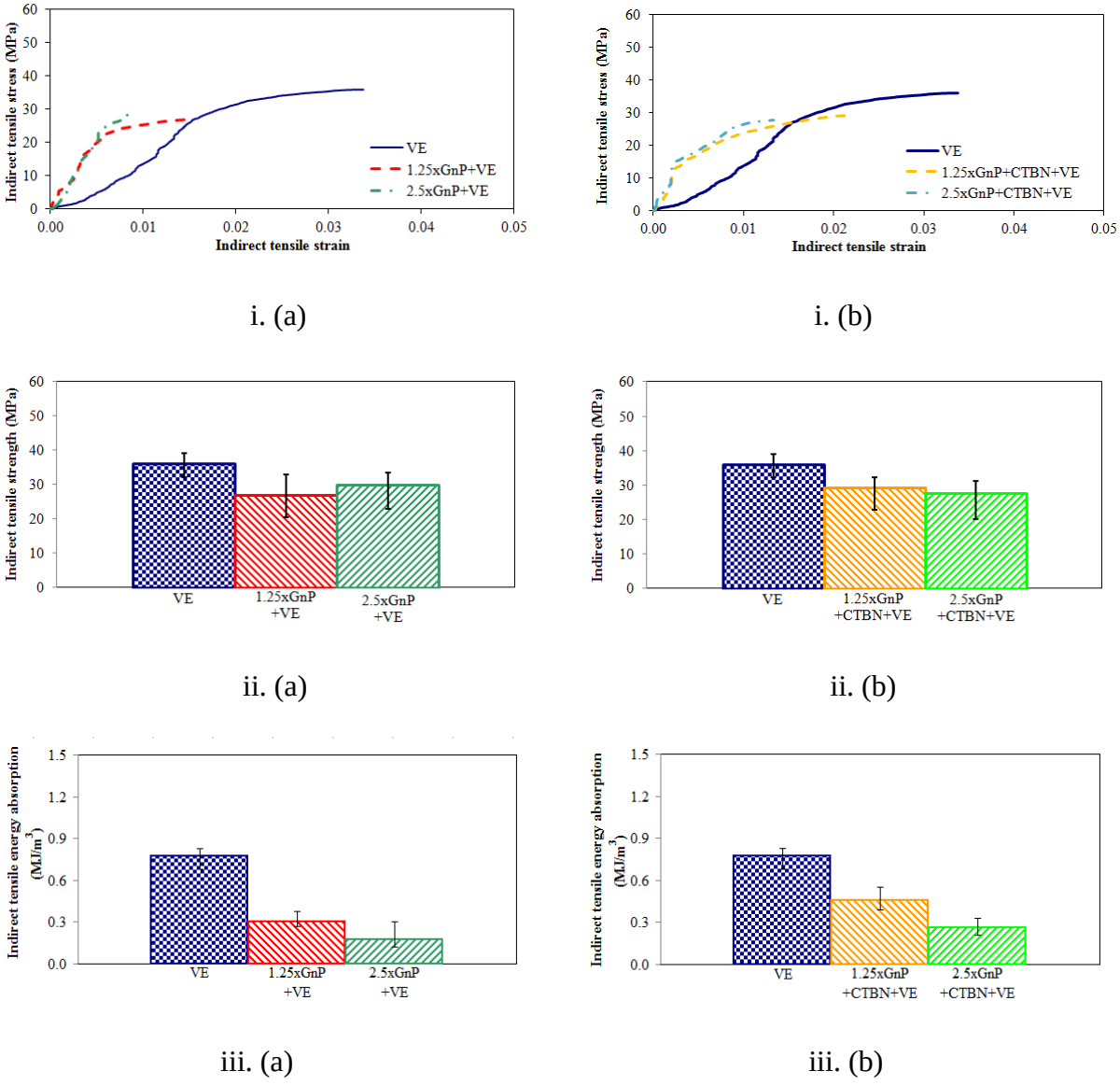

Figure 3.5: Quasi-static indirect tensile response (i) typical stress vs. strain behavior, (ii) strength, and (iii) energy absorbing capacity of; (a) graphite platelet reinforced, and (b) with additional CTBN toughened vinyl ester nanocomposites [note: pure vinyl ester specimens did not fail within the 10 kN load cell limit of test equipment used for quasi-static testing]

strength and failure strain data for pristine vinyl ester as reported in Table 3.1 are not meaningful. However, addition of xGnP and CTBN makes the vinyl ester polymer more brittle (Figure 2.13-c) and thus suitable for this indirect experimental test method. The quasi-static indirect tensile

response (Table 3.1) agrees reasonably with previous investigations performed [32] according to ASTM 638-08 [31], using dog-bone specimen geometry (Table 1.1).

The quasi-static indirect tensile stress-strain history for pure vinyl ester, xGnP reinforced and CTBN toughened samples are shown in Figure 3.5. As mentioned earlier, stress-strain plots for only the pure vinyl ester specimens have been terminated due to load cell capacity before the specimen failure occurs, whereas reinforced samples failed within the load cell range of 10 kN.

It can be observed in Figure 3.5-ii that tensile strength of pure vinyl ester is reduced by the addition of xGnP reinforcement (Figure 3.5-ii-a), and even with CTBN toughening (Figure 3.5-ii-b). Energy absorbing capacity (Figure 3.5-iii) is similarly affected by the addition of xGnP (Figure 3.5-iii-a). The addition of CTBN did not improve the energy absorbing capacity (Figure 3.5-iii-b) of pure vinyl ester, however, a marginal enhancement (Figure 3.5-iii-b) can be observed when compared to only xGnP reinforced (i.e., without CTBN, Figure 3.5-iii-a) nanocomposites.

3.4. Strain rate effect

Observation of Figure 3.5 with Figure 3.4 shows the strain-rate dependency of tensile strength and energy absorbing capacity of these candidate materials. As noted earlier, during quasi-static tests pure vinyl ester did not fail within maximum load limit of the load cell used, deforming elliptically in a ductile manner (Figure 2.13-b and Figure 3.5-i). However, it failed in a brittle fashion at much lesser strain (Figure 3.4-i) under the high-strain rate SHPB loading. This ductile-to-brittle transition may be due to the significant influence of strain-rate effect. These nanocomposites can be considered as thermo-viscoelastic under high-strain rate loading in Hopkinson bar experiments, and the time-temperature superposition principle would

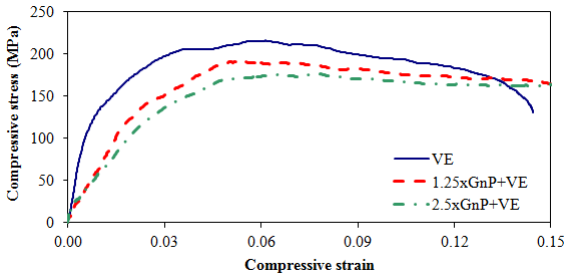

i. (a)

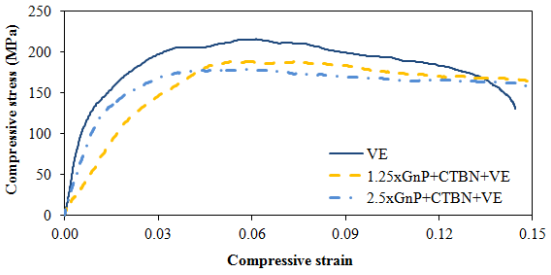

i. (b)

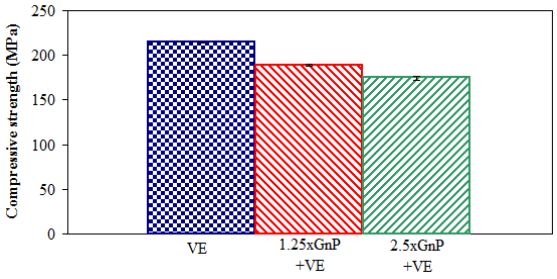

ii. (a)

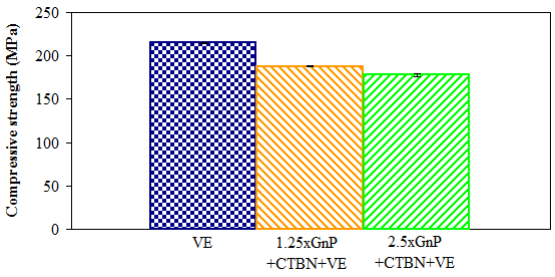

ii. (b)

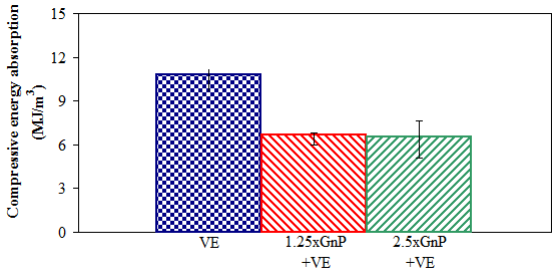

iii. (a)

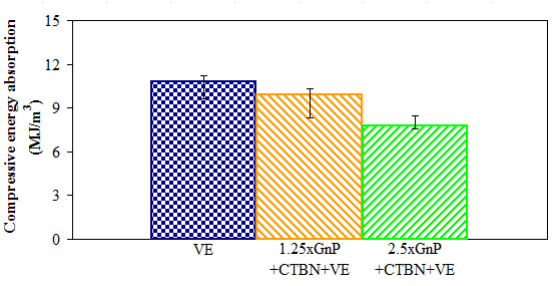

iii. (b)

Figure 3.6: High-strain rate compressive response from SHPB tests (i) typical stress vs. strain behavior, (ii) strength, and (iii) energy absorbing capacity of; (a) graphite platelet reinforced, and (b) with additional CTBN toughened vinyl ester nanocomposites

be applicable for characterizing their response. A higher strain rate would correspond to a shorter loading time, equivalent to lower temperatures [52] causing the ductile-to-brittle transition of the specimen. This phenomenon has been further explained by the authors applying a technique of measuring fractal parameters of the fractured surfaces on the same candidate materials [41].

About 25% increment in tensile strength is observed at high-strain rate loading (Figure 3.4-ii) with respect to the quasi-static response (Figure 3.5-ii). The energy absorption capacity of pure vinyl ester is adversely affected under high-strain rate loading, whereas it is improved with the addition of xGnP reinforcement (Figures 3.5-iii-a and 3.4-iii-a). However, additional CTBN toughening agent could not contribute towards increasing the energy absorbing capacity (Figure 3.5-iii-b and 3.4-iii-b).

3.5. Dynamic compressive response

Figure 3.6 shows dynamic compressive response of the candidate materials tested at similar strain-rate of about 1000 s^{-1}. It can be observed in Figure 3.6-ii that tensile strength of pure vinyl ester is reduced gradually by the addition of xGnP reinforcement (Figure 3.6-ii-a), and even with CTBN toughening (Figure 3.6-ii-b). Energy absorbing capacity (Figure 3.6-iii) is similarly affected by the addition of xGnP (Figure 3.6-iii-a). The addition of CTBN did not improve the energy absorbing capacity (Figure 3.6-iii-b) of pure vinyl ester, however, a marginal enhancement (Figure 3.6-iii-b) is observed when compared to only xGnP reinforced (i.e., without CTBN, Figure 3.6-iii-a) nanocomposites.

3.6. Comparative study of dynamic tensile and compressive responses

Comparative observation of Figures 3.3 and 3.4 with Fig. 3.6 indicates that the stress–strain behavior of these candidate materials under dynamic tension differs significantly from its dynamic compressive behavior. The compressive strength (Figure 3.6-ii) of the candidate materials is observed to be about 300% more than tensile strength under high-strain rate loading (Figures 3.3-ii and 3.4-ii). The energy absorption capacity is also significantly higher (about

2000%) under dynamic compressive loading (Figure 3.6-iii) than under dynamic tensile loading (Figures 3.3-iii and 3.4-iii). It is evident that these vinyl ester based nanocomposites are brittle at high strain rates. The nano-reinforcement and additional toughening, although is detrimental to the properties under dynamic compression, a minimal improvement is observed in dynamic tension.

CHAPTER IV CONCLUSION AND RECOMMENDATIONS

4.1. High strain rate tensile test techniques

Two modified tensile test methods are proposed for the high-strain rate dynamic characterization of high stiffness and low strength xGnP and CTBN reinforced vinyl ester nanocomposites. Significant features of the proposed techniques include –

- The SHPB reverse impact technique is implemented and specimen geometry is optimized for high-strain rate dynamic characterization of the candidate materials under uniaxial tensile loading.
- Due to the very low transmitted pulse signal, an alternative approach (using incident pulse and quasi-static properties of the candidate materials) is adopted for estimating stress-time history. The transmission bar may also be modified with a low impedance material and/or smaller cross-sectional area for obtaining true dynamic tensile stress.
- SHPB system is customized to test Brazilian disk specimens for obtaining indirect tensile response of the candidate materials under high-strain rate dynamic loading.
- Considering Brazilian disk specimen simplifies the complex geometry of conventional direct tensile test specimen, and the loading fixture. The two concave end loading fixtures assembled in between the incident and transmission bars of SHPB system ensures easy, secure and self-aligned gripping of the disk specimen.

- High-speed digital photography diagnosis validates the specimen failure mechanism in this indirect test method for characterizing the tensile properties of graphite platelet reinforced and additionally CTBN toughened vinyl ester nanocomposites.
- Considering the Brazilian disk diameter as effective gage length is found to be more convenient for transverse strain measurement than the centrally concentrated gage length.
- Complexities of conventional strain gage application for measuring the transverse diametrical expansion of disk specimens under high-strain rate diametrical compressive loading are overcome by using a non-contact Laser Occluding Expansion Gage.
- The conventional Brazilian disk test method could not capture true behavior of the apparently ductile pure vinyl ester under quasi-static loading.

4.2. Indirect tensile tests and strain rate effect

Quasi-static and dynamic experimental investigations characterized the contribution of xGnP reinforcement along with CTBN toughening on the tensile properties of vinyl ester based nanocomposites and the effect of strain rate. The key observations in this investigation are -

- Tensile strength and energy absorbing capacity of pure vinyl ester is reduced by the addition of xGnP reinforcement and even with CTBN toughening under quasi-static loading.
- Addition of CTBN marginally improved the energy absorbing capacity of the only xGnP reinforced (without CTBN) nanocomposites under quasi-static loading.
- Tensile strength of pure vinyl ester remains almost the same with addition of xGnP reinforcement and even with CTBN toughening under high-strain rate loading.
- Energy absorbing capacity of pure vinyl ester is improved with addition of xGnP reinforcement under high-strain rate loading.

- Pure vinyl ester shows ductile-to-brittle transition from quasi-static to high-strain rate loading.
- Tensile strength obtained in quasi-static test is increased under high strain-rate loading for these candidate nanocomposites.
- The energy absorption capacity of pure vinyl ester is adversely affected under high-strain rate loading.

4.3. Comparison of dynamic tensile and compressive response

The differences of the properties under tensile and compressive loading are presented. The key observations in this investigation are –

- The stress-strain behavior of the candidate materials under dynamic tension differs significantly from its dynamic compressive behavior.
- Reinforcing vinyl ester with xGnP and toughening with CTBN is found to be detrimental to the properties of candidate nanocomposites under dynamic compression, although a minimal improvement of these properties is observed in dynamic tension.

4.4. Recommendations for future work

The recommendations on the existing direct tensile SHPB system for obtaining more accurate stress-time history of materials similar to this research are as follows –

- An aluminum hollow striker bar can be used, instead of the existing steel hollow bar, for avoiding impedance mismatch within SHPB system.
- A hollow transmission bar [45] can be considered, instead of the existing solid one, for improving the amplitude of transmission pulse.

- A suitable noise filtering algorithm can be applied to the LOEG response. This may help in improving accuracy of capturing the instantaneous change of tensile strain rate due to initiation of failure.
- Identifying the time of specimen failure-instant is crucial for obtaining ultimate-strain and strength of materials at high-strain rate tensile testing. The existing LOEG can be customized for capturing the simultaneous events of transverse diameter expansion and initiation of splitting at the disk specimen center.
- The key dynamic fracture parameters, including fracture initiation toughness, fracture energy, fracture propagation toughness, and fracture velocity of the toughened nanocomposites and cementitious materials can be measured [47] by suitable adaptation of SHPB, Brazilian disk and LOEG.
- Ultra-high speed digital photography along with speckle metrology can be applied for investigating non-uniform specimen deformation and failure mechanisms of test specimens subjected to high-strain rate loading.

REFERENCES

1. Hopkinson, B., 1914, “A Method of Measuring The Pressure Produced in The Detonation of High Explosives or by The Impact of Bullets,” Philosophical Transactions of the Royal Society of London. Series A, Containing Papers of a Mathematical or Physical Character, 213, pp. 437-456.

2. Kolsky, H., 1949, “An Investigation of The Mechanical Properties of Materials at Very High Rates of Strain,” Proceedings of the Physical Society. Section B, 62, pp. 676-700.

3. Harding, J., Wood, E.O., Campbell, J.D., 1960, “Tensile Testing of Materials at Impact Rates of Strain,” J. Mech. Eng. Sci., 2(2), pp. 88-96.

4. Lindholm, U.S., Yeakley, L.M., 1968, “High Strain-Rate Testing: Tension and Compression,” Experimental Mechanics, 8(1), pp. 1-9.

5. Albertini, C., Montagnani, M., 1974, “Mechanical Properties at High Rates of Strain,” Institute of Physics, London, pp. 22.

6. Staab, G.H., Gilat, A., 1991, “A Direct-Tension Split Hopkinson Bar for High-Strain Rate Testing,” Experimental Mechanics, 31(3), pp. 232-235.

7. Cadoni, E., Solomos, G., Albertini, C., 2009, “Mechanical Characterization of Concrete in Tension and Compression at High Strain Rate Using a Modified Hopkinson Bar,” Magazine of concrete research, 61(3), pp. 221-230.

8. Nicholas, T., 1980, “Tensile Testing of Materials at High Rates of Strain,” Experimental Mechanics, 21(5), pp. 177-185.

9. Kawata, K., Hashimoto, S., Kurokawa, K., Kanayama, N., 1979, “A New Testing Method for The Characterization of Materials in High-Velocity Tension,” The Institute of Physics. S. No. 47, Ch. 1, pp. 71-80.

10. Li, M., Wang, R., Han, M. B., 1993, “A Kolskey Bar: Tension, Tension-Tension,” Experimental Mechanics, 33(1), pp. 7-14.

11. Owens, A. T., Tippur, H. V., 2009, “A Tensile Split Hopkinson Bar for Testing Particulate Polymer Composites under Eelevated Rates of Loading,” Experimental Mechanics, 47, pp. 799-811.

12. Gilat, A., Goldberg, R. K., Roberts, G. D., 2005, “Strain Rate Sensitivity of Epoxy Resin in Tensile and Shear Loading,” NASA/TM—2005-213595, pp. 1-33.

13. Chen, R., Dai, F., Lu, L., Lu, F., Xia, K., 2010, “Determination of Dynamic Tensile Properties for Low Strength Brittle Solids,” Experimental and Applied Mechanics, 6, pp. 321-326.

14. Rajendran, A. M., Bless, S. J, 1986, “Determination of Tensile Flow Stress Beyond Necking at Very High Strain Rate,” Experimental Mechanics, 26(4), pp. 319-323.

15. Melin, L.G., Stahle, P., Sundin, K. G., 1998, “High Strain Rate Tensile Using Microscopic High Speed Photography,” 11th International Conference on Experimental Mechanics, pp. 175-179.

16. Sharma, A., Shukla, A., Prosser, R. A., 2002, “Mechanical Characterization of Soft Materials Using High Speed Photography and Split-Hopkinson Pressure Bar Technique,” Journal of Materials Science, 37, pp. 1005-1017.

17. Vinyl ester resin, Article id 986, Resin systems for use in fiber-reinforced composite materials. www.azom.com, Source: SP Systems, Date Added: Oct 25, 2001, Updated: Jun 11, 2013.

18. Ashland Inc., 2011, “DERAKANE 510A-40 Epoxy Vinyl Ester Resin,” Technical Datasheet, Document 1775V2 F2, Language EN V1, Approved 2008-9-8, pp. 1-4.

19. Shivakumar, K. N., Swaminathan, G., Sharpe, M. “Carbon vinyl ester composites for enahanced performance in marine applications”, Journal of Reinforced Plastics and Composites, 25(10), 2006

20. Chung, D. D. L., 1987, “Exfoliation of Graphite,” Journal of Material Science, 22(12), pp. 4190-4198.

21. Yoshida, A., Hishiyama, Y., Inagaki, M., 1991, “Exfoliated Graphite from Various Intercalation Compounds,” J. Carbon, 29(8), pp. 1227 – 1231.

22. Giannelis, E. P., 1996, “Polymer Layered Silicate Nanocomposites”, Journal of Advanced Materials, 8(1), pp. 29–35.

23. Auad, M. L. P., Frontini, M., Borrajo, J., Aran-guren, M. I., 2001, “Liquid Rubber Modified Vinyl Ester Resins: Fracture and Mechanical Behavior,” Polymer, 42(8), pp. 3723-3730.

24. Celzard, A., Schneider, S., Mareche, J. F., 2002, “Densificaton of Expanded Graphite,” J. Carbon, 40, pp. 2185–2191.

25. Toshiaki, E., Masatsugu, S., Morinobu, E., 2003, “Graphite Intercalation Compounds and Applications,” Oxford University Press, Inc. New York.

26. Fröhlich, J., Thomann, R., Mülhaupt, R., 2003, “Toughened Epoxy Hybrid Nanocomposites Containing Both an Or-ganophilic Layered Silicate Filler and a Compatibilized Liquid Rubber,” Macromolecules, 36(19), pp. 7205-7211.

27. Yasmin, A., Daniel, I., 2004, “Mechanical and Thermal Properties of Graphite Platelet/Epoxy Composites,” J. Polymer, 45(24), pp. 8211-8219.

28. Fukushima H., and Drzal L.T., 2004, “Graphite Nanoplatelets as Reinforcement for Polymers: Structural and Electrical Properties,” Proceedings of 17th international conference on American Society for composites.

29. Balakrishnan, S., Start, P. R., Raghavan, D., Hud-son, S. D., 2005, "The Influence of Clay and Elastomer Concentration on the Morphology and Fracture Energy of Preformed Acrylic Rubber Dispersed Clay Filled Epoxy Nanocomposites," Polymer, 46(25), pp. 11255- 11262.

30. Drzal, L.T., Fukushima, H., 2006, "Exfoliated Graphite Nanoplatelets (xGnP): A Carbon Nanotube Alternative. The Nanotechnology Conference, Boston, May 7-11, 2006.

31. ASTM Standard D 638-08, 2008, "Standard Test Method for Tensile Properties of Plastics", ASTM International.

32. Magableh, A., 2010, "Viscoelastic and shock response of nanoclay and graphite platelet reinforced vinyl ester nanocomposites," PhD Dissertation, Dept. of Mechanical Engineering, University of Mississippi.

33. ASTM Standard D 6641/D 6641M, 2007, "Standard Test Method for Determining the Compressive Properties of Polymeric Matrix Composite Laminates Using a Combined Loading Compression (CLC) Test Fixture," ASTM International.

34. Pramanik, B., Mantena, P. R., 2012, "Energy Absorption of Nano-Reinforced and Sandwich Composites in Ballistic and Low-Velocity Punch-Shear" Open Journal of Composite Materials, 2(3), pp. 87-96.

35. Mantena, P. R., Cheng, A. H. D., Al-Ostaz, A., Rajendran, A. M., 2010, (Grant # N00014-7-1-1010) "Blast and Impact Resistant Composite Structures for Navy Ships," Proceedings of Marine Composites and Sandwich Structures, 2010, Office of Naval Research – Solid Mechanics Program Review, Adelphi, MD, Sep 27-29, 2010.

36. Ferry, J. D., 1980, "Viscoelastic Properties of Polymers", 3rd Edition, John Wiley & Sons Inc., New York.

37. Pramanik, B., Mantena, P. R., 2011, "Viscoelastic Response of Graphite Platelet and CTBN Reinforced Vinyl Ester Nanocomposites," Materials Sciences and Applications, 2(11), pp. 1667-1674.

38. ASTM Standard D-4065-01, "Standard Practice for Plastics: Dynamic Mechanical Properties: Determination and Report of Procedure," ASTM International, 2000.

39. TA Instruments, 2004, "Dynamic Mechanical Analyzer, Q SeriesTM, Getting Started Guide," Revision F, New Castle, http://www.adhesivesmag.com.

40. ASTM Standard: D3763-06, 2006, "Standard Test Method for High Speed Puncture Properties of Plastics Using Load and Displacement Sensors," ASTM International, D20 Plastics D20.10 Mechanical Properties, September 2006.

41. Pramanik, B., Tadepalli, T., Mantena, P. R., 2012, "Surface Fractal Analysis for Estimating the Fracture Energy Absorption of Nanoparticle Reinforced Composites" Materials, 2012, (submitted on Mar 16, 2012, under review).

42. Lu, C., 2007, “Some Notes on The Study of Fractals in Fracture,” 5th Australasian Congress on Applied Mechanics, ACAM 2007, Brisbane, Australia, December 10-12, 2007, 234-239.

43. Lair, J., and Hui, D., 2010, “High Strain Rate Compression Tests on Nanocomposite Samples Using a Split-Hopkinson Bar,” Internal report, ONR Sub-award # 4500188784 for Blast and Impact Resistant Composite Structures for Navy Ships, University of Mississippi.

44. Lair, J., 2011, High strain rate tensile tests on nanocomposite samples using a split-Hopkinson bar, performed at CAVS facility, Starkville, MS on July 8, 2011.

45. Carneiro, F., Barcellos, A., 1953, “International Association of Testing and Research Laboratories for Materials and Structures” Rilem Bulletin, 13, pp. 99-125.

46. Akazawa, T., 1953, “Tension Test Method for Concretes - International Association of Testing and Research Laboratories for Materials and Structures” Rilem Bulletin, 13, pp. 13-23.

47. Thimoshenko, S., Goodier, J. N., 1951, “Section 37. Stresses in a Circular Disk” Theory of Elasticity, McGraw-Hill Book Co., Inc., pp. 107-111.

48. John, R., Antoun, T., A.M. Rajendran, 1991, "Effect of Strain Rate and Size on Tensile Strength of Concrete," American Physical Society - Shock Compression of Condensed Matter 1991, Elsevier Science Publishers, pp. 501-504.

49. Ramesh, K.T., Narsimhan, S., 1996, “Finite Deformations and the Dynamic Measurement of Radial Strains in Compression Kolsky Bar Experiments”, Int. J. Solids Structures, 33(25), pp. 3723-3738.

50. Chen, R., Dai, F., Qin, J., Lu, F., 2013, “Flattened Brazilian Disc Method for Determining the Dynamic Tensile Stress-Strain Curve of Low Strength Brittle Solids”, Experimental Mechanics, doi: 10.1007/s11340-013-9733-6.

51. Song, B., Connelly, K., Korellis, J., Lu, W.-Y., Antoun, B.R., 2009, “Improvements in Kolsky-bar design for mechanical characterization of materials at high strain rates”, Measurement Science and Technology, 20(11), 115701, doi:10.1088/0957-0233/20/11/115701

52. Chen, W., Lu, F., Zhou, B., 2000, “A Quartz-Crystal Embedded Split Hopkinson Pressure Bar for Soft Materials,” Experimental and Applied Mechanics, 40(1), pp. 1-6.

53. Precision Ground Bars, Grinding Services – Boston Centerless, www.bostoncenterless.com.

54. Awaji, H., Sato, S., 1979, “Diametral Compressive Testing Method”, Journal of Engineering Materials and Technology, 101, pp. 139-147.

55. Wang, Q. Z., Jia, X. M., Kou, S. Q., Zhang, Z. X., Lindqvist, P. A., 2004, “The Flattened Brazilian Disc Specimen Used for Testing Elastic Modulus, Tensile Strength and Fracture

Toughness of Brittle Rocks: Analytical And Numerical Results", International Journal of Rock Mechanics & Mining Sciences 41, pp. 245–253.

56. Frew, D. J., Forrestal, M. J., Chen, W., 2002, "Pulse Shaping Techniques for Testing Brittle Materials with a Split Hopkinson Pressure Bar", Experimental Mechanics, 42(1), pp. 93-106.

57. Wertheimer, 1912, "Experimentelle Studien über das Sehen von Bewegung", Zeitschrift für Psychologie 61, pp. 161–265.

58. Jianhong, Y., Wu, F.Q., Sun, J.Z., 2009, "Estimation of the tensile elastic modulus using Brazilian disc by applying diametrically opposed concentrated loads", International Journal of Rock Mechanics & Mining Sciences, 46, pp. 568–576.

59. Yi, F., Zhu, Z., Zu, F., Hu, S., Yi, P., 2001, "Strain Rate Effects on the Compressive Property and the Energy-Absorbing Capacity of Aluminum Alloy Foams", Materials Characterization, 47, pp. 417-422.

VITA

Brahmananda 'Brahma' Pramanik
Voice: (662) 202-2286
E-mail: bpramanik75@gmail.com
Web: http://www.linkedin.com/in/bpramanik

EDUCATION	Ph.D., Mechanical Engineering University of Mississippi - University, MS, USA Dissertation: High-Strain Rate Tensile Characterization of Graphite Platelet Reinforced Vinyl Ester Nanocomposites adapting split-Hopkinson Pressure Bar	2013
	M.S., Mechanical Engineering University of Mississippi - University, MS, USA Thesis: Punch-Shear and Ballistic Energy Absorption Characteristics of Nano-reinforced Panels, Laminated Face Sheets and Sandwich Composites	2010
	B.S., Mechanical Engineering Institution of Engineers (India), Kolkata, India	2006
	A.S., Mechanical Engineering West Bengal State Council of Technical Education, Kolkata, India	1997
EXPERIENCE	Graduate Teaching/Research Assistant Blast and Impact Dynamics Laboratory Dept. of Mechanical Engineering University of Mississippi - University, MS, USA	2007 - Present
	Project Assistant Composite Application Laboratory Collaboration - Depts. of Mechanical, Chemical and Aerospace Engineering – TIFAC/DST Indian Institute of Technology - Kharagpur, India	2004 – 2007

	CAD Specialist Ship Classification and Maintenance Project American Bureau of Shipping (ABS), USA, Regal Services – Kolkata, India	2002 – 2004
	CAD Specialist DPS Technologies – Kolkata, India	2001 – 2002
	Junior Design Engineer Engineering and Machinery Division GKW Ltd – Howrah, WB, India	1997 – 2001

HONORS AND AWARDS	▪ Senator of Mechanical Engineering, Graduate Student Council, University of Mississippi	2013
	▪ Dean's Fellowship, University of Mississippi	2013
	▪ ERDC-CERL Research Assistantship	2012 – 2014
	▪ ONR Research Assistantship, Composite Structure and Nano-Engineering Research	2007 – 2011
	▪ NSF Travel Award, Micro & Nanotechnology Forum, ASME-IMECE2012	2012
	▪ Academic Scholarship Award, WBBSE, India	1992

SOCIETY MEMBERSHIPS ASME | NSBE | GBP | IEI

JOURNAL PUBLICATIONS

Mantena, P.R.; Pramanik, B; Tadepalli, T; Boddu, V. M.; Brenner, M. W.; Kumar, A., (2014) Effect of Process Parameters on the Dynamic Modulus, Damping and Energy Absorption of Vertically Aligned Carbon Nano-Tube (VACNT) Forest Structures, Journal of Multifunctional Composites, Vol. 2(2), pp. 93-100, doi:10.12783/issn. 2168-4286/2.2/Mantena

Pramanik, B.; Mantena, P.R., (2014) Strain Rate Dependent Ductile-to-Brittle Transition of Graphite Platelet Reinforced Vinyl Ester Nanocomposites, Advances in Materials Science and Engineering, Volume 2014 (2014), Article ID 765698, 8 pages, doi: 10.1155/2014/765698

Mantena, P.R.; Tadepalli, T.; Pramanik, B.; Boddu, V.M.; Brenner, M.W.; Stephenson, L.D.; and Kumar, A., (2013) Energy Dissipation and the High-Strain Rate Dynamic Response of Vertically Aligned Carbon Nanotube (VACNT) Ensembles Grown on Silicon Wafer Substrate, Journal of Nanomaterials, Vol. 2013, Article id 259458, 7 pages, doi:10.1155/2013/259458.

Pramanik, B.; and Mantena, P.R. (2012) Energy Absorption of Nano-Reinforced and Sandwich Composites in Ballistic and Low-Velocity Punch-Shear, Open Journal of Composite Materials, Vol. 8(1), pp. 87-96, doi:10.4236/ojcm.2012.23010.

Pramanik, B.; Tadepalli, T.; and Mantena, P.R. (2012) Surface Fractal Analysis for Estimating the Fracture Energy Absorption of Nanoparticle Reinforced Composites, Materials, Vol. 5, pp. 922-936, doi:10.3390/ma5050922.

Pramanik, B.; and Mantena, P.R. (2011), Viscoelastic Response of Graphite Platelet and CTBN Reinforced Vinyl Ester Nanocomposites, Materials Sciences and Applications, Vol. 2, pp. 1667-1674, doi:10.4236/msa.2011.211222.

Pramanik, B.; and Mantena, P.R. (2009) Punch-Shear Characteristics of Nanoclay and Graphite Platelet Reinforced Vinyl Ester Plates, Laminated Face Sheets and Sandwich Composites under Low Velocity Impact, ASME 2009 Early Career Technical Journal, Vol. 2(3), pp. 56-63.

Pramanik, B.; and Mantena, P.R.; and Rajendran, A.M., High-Strain Rate Tensile and Compressive Characterization of Graphite Nanoplatelet Reinforced Vinyl Ester Composites, Experimental Mechanics, (under review)

Pramanik, B.; Mantena, P.R.; Tadepalli, T.; and Rajendran, A.M., Indirect Tensile Characterization of Graphite Platelet Reinforced Vinyl Ester Nanocomposites at High-Strain Rate, Open Journal of Composite Materials, (Submitted)

CONFERENCE PROCEEDINGS

Pramanik, B.; Mantena, P.R.; and Rajendran, A.M., High-Strain Rate Tensile Characterization of Vinyl Ester Nanocomposite and Cementitious Materials, Micro & Nanotechnology Forum, ASME International Mechanical Engineering Congress & Exposition (ASME-IMECE), Houston, TX, Nov 9-15, 2012.

Pramanik, B.; Tadepalli, T.; and Mantena, P.R., Estimation of Fracture Energy Absorption Based on Fractal Surface Analysis of Nano-Composites Subjected to Low Velocity Impact, Mid-south Annual Engineering and Sciences Conference (MAESC), Memphis, TN, May 3, 2011.

Pramanik, B.; and Mantena, P.R., Low Velocity Punch-Shear Response of Nanoclay and Graphite Platelet Reinforced Vinyl Ester Plates, Laminated Face Sheets and Sandwich Composites, ASME 2009 International Mechanical Engineering Congress and Exposition, Vol. 11: Mechanics of Solids, Structures and Fluids, Lake Buena Vista, Florida, USA, November 13–19, 2009.

Pramanik, B.; and Mantena, P.R., Punch-Shear Characteristics of Nanoclay and Graphite Platelet Reinforced Vinyl Ester Plates, Laminated Face Sheets and Sandwich Composites under Low Velocity Impact, ASME Early Career Technical Conference (ASME-ECTC 2009), Tuscaloosa, AL, Oct 2-3, 2009.

Pramanik, B.; and Mantena, P.R., Punch-Shear Response of Nanoclay and Graphite Platelet Reinforced Vinyl Ester Nanocomposites Under Low Velocity Impact, Mid-south Annual Engineering and Sciences Conference (MAESC), Memphis, TN, May 5, 2009.